1997

Computer simulation of grain growth in HAZ.

Jinhua Gao
University of Alabama at Birmingham

INFORMATION TO USERS

This manuscript has been reproduced from the microfilm master. UMI films the text directly from the original or copy submitted. Thus, some thesis and dissertation copies are in typewriter face, while others may be from any type of computer printer.

The quality of this reproduction is dependent upon the quality of the copy submitted. Broken or indistinct print, colored or poor quality illustrations and photographs, print bleedthrough, substandard margins, and improper alignment can adversely affect reproduction.

In the unlikely event that the author did not send UMI a complete manuscript and there are missing pages, these will be noted. Also, if unauthorized copyright material had to be removed, a note will indicate the deletion.

Oversize materials (e.g., maps, drawings, charts) are reproduced by sectioning the original, beginning at the upper left-hand corner and continuing from left to right in equal sections with small overlaps. Each original is also photographed in one exposure and is included in reduced form at the back of the book.

Photographs included in the original manuscript have been reproduced xerographically in this copy. Higher quality 6" x 9" black and white photographic prints are available for any photographs or illustrations appearing in this copy for an additional charge. Contact UMI directly to order.

UMI

A Bell & Howell Information Company
300 North Zeeb Road, Ann Arbor MI 48106-1346 USA
313/761-4700 800/521-0600

COMPUTER SIMULATION OF GRAIN GROWTH IN HAZ

by

JINHUA GAO

A DISSERTATION

Submitted to the graduate faculty of The University of Alabama at Birmingham,
in partial fulfillment of the requirements for the degree of
Doctor of Philosophy

BIRMINGHAM, ALABAMA

1997

ABSTRACT OF DISSERTATION
GRADUATE SCHOOL, UNIVERSITY OF ALABAMA AT BIRMINGHAM

Degree Doctor of Philosophy Program Materials Engineering

Name of Candidate Jinhua Gao

Committee Chair Raymond G. Thompson

Title Computer Simulation of Grain Growth in HAZ

Two different models for Monte Carlo simulation of normal grain growth in metals and alloys were developed. Each simulation model was based on a different approach to couple the Monte Carlo simulation time to real time-temperature. These models demonstrated the applicability of Monte Carlo simulation to grain growth in materials processing.

A grain boundary migration (GBM) model coupled the Monte Carlo simulation to a first principle grain boundary migration model. The simulation results, by applying this model to isothermal grain growth in zone-refined tin, showed good agreement with experimental results.

An experimental data based (EDB) model coupled the Monte Carlo simulation with grain growth kinetics obtained from the experiment. The results of the application of the EDB model to the grain growth during continuous heating of a beta titanium alloy correlated well with experimental data.

In order to acquire the grain growth kinetics from the experiment, a new mathematical method was developed and utilized to analyze the experimental data on isothermal grain growth. Grain growth in the HAZ of 0.2% Cu-Al alloy was successfully simulated using the EDB model combined with grain growth kinetics obtained from the

experiment and measured thermal cycles from the welding process. The simulated grain size distribution in the HAZ was in good agreement with experimental results.

The pinning effect of second phase particles on grain growth was also simulated in this work. The simulation results confirmed that by introducing the variable R, degree of contact between grain boundaries and second phase particles, the Zener pinning model can be modified as

$$\frac{D}{r} = \frac{K}{Rf}$$

where D is the pinned grain size, r the mean size of second phase particles, K a constant, f the area fraction (or the volume fraction in 3-D) of second phase.

ACKNOWLEDGMENTS

I would like to express my sincere gratitude to my advisor, Dr. Raymond G. Thompson, for giving me the opportunity to make my dream true, for his guidance and help throughout this research work, and for everything he did for me.

I would like to express my grateful appreciation to my dissertation committee member, Dr. Burton Patterson, for his fruitful discussions and good comments on this research work. I would also like to express my appreciation to my other committee members, Drs. Barry Andrews, Gregg Janowski, and Viola Acoff, for their valuable input and help. The appreciation is extended to other members of the faculty and staff in the Department of Materials and Mechanical Engineering and my fellow students in the Welding Lab, Mr. Curt Malam and Mr. Brett Boutwell, for their assistance. The assistance from the Department of Materials Science and Engineering, University of Alabama, in rolling samples is also appreciated.

I would like to give my special thanks to my wife, Na Wu, and my son, Xin. Without their love and encouragement, I would not have been able to complete my degree works.

Finally, I would like to acknowledge the National Science Foundation for their financial support of this research under grants No. DMR-9112251 and No. DMR-9417326.

TABLE OF CONTENTS

Page

ABSTRACT ii

ACKNOWLEDGMENTS iv

LIST OF TABLES vii

LIST OF FIGURES viii

INTRODUCTION 1
Grain Growth Kinetics 1
Empirical grain growth kinetics 1
Parabolic grain growth kinetics 1
Power law of grain growth kinetics 2
Topological analysis of grain growth 3
Mean field theories 5
Grain growth as dislocation climb 6
Experimental Results on Grain Growth Kinetics 7
Zener Pinning 8
Monte Carlo Simulation Technique 10
Thermal Field in HAZ 13
Models for Grain Growth in HAZ 14
Ashby-Easterling's model 14
Alberry-Chew-Jones's model 16
The Goals of the Present Work 18

EXPERIMENTAL PROCEDURES 26
Sample Preparation 26
Isothermal Grain Growth 26
Metallographic Sample Preparation 26
Welding Experiments 27
Grain Size Measurement 28
Calculation of the Degree of Contact Between
Grain Boundaries and Second Phase Particles 29
Monte Carlo Simulations 30
Grain boundary migration (GBM) model 30
Experimental data based (EDB) model 32

TABLE OF CONTENTS (Continued)

Page

Monte Carlo simulation of Zener pinning 33
Monte Carlo simulation of grain growth in the weld HAZ 34

EXPERIMENTAL RESULTS 39
Grain Growth Kinetics 39
Welding Experiments 42
Simulations of Grain Growth 43
Application of the GBM model to isothermal grain growth in zone-refined tin 43
Application of the EDB model to the heat treatment of a titanium alloy (continuous heating) 43
Application of the EDB model to grain growth in HAZ of 0.2% Cu-Al alloy 44
Grain growth with Zener pinning of second phase particles 45

DISCUSSION 70
Selection of Monte Carlo Simulation System 70
Application of the Two Models 71
Description of Grain Size in HAZ 72
Modification of Zener Pinning Model 73
Comparison of Modified Zener Pinning Model with Simulation Results 75

CONCLUSIONS 80

REFERENCES 82

LIST OF TABLES

Table		Page
1	Experimental results of time exponent in grain growth kinetics	7
2	Chemical compositions of the experimental alloy (wt%)	26
3	Heat treatment for grain growth kinetics	27
4	Experimental results on grain growth kinetics of 0.2% Cu-Al	40
5	Results of grain growth kinetics analysis for 0.2% Cu-Al	41

LIST OF FIGURES

Figure		Page
1	The 4-rayed vertex tends to decompose to two 3-rayed vertices	19
2	2-D grain structure evolution (after [5])	20
3	Grain size distribution (after [1])	21
4	Temperature dependence of the time exponent in isothermal grain growth	22
5	Triangular simulation matrix	23
6	A diagram for a 2% Cr-Mo steel, thick plate, T_0 = 300K (after [73])	24
7	Comparison of calculated grain size to experiment data (after [75])	25
8	Experimental welding set-up	35
9	The locations of thermocouples on the sample surface	36
10	Intersection of second phase particles and grain boundaries	37
11	Configuration of second phase particles in the simulation matrix	38
12	The assumed time offset, τ	48
13	The deviation function as a function of assumed time offset, 0.2% Cu-Al	49
14	Determination of K_0 and Q in grain growth kinetics, 0.2% Cu-Al	50
15	Isothermal grain growth kinetics, 0.2% Cu-Al	51
16	The thermal cycles in the HAZ of 0.2% Cu-Al plate, GTAW welding, arc speed: 7.5 ipm, power input: 760 W	52
17	The peak temperature gradient in the HAZ of 0.2% Cu-Al	53
18	Real grain structure in the weld of 0.2% Cu-Al	54

LIST OF FIGURES (Continued)

Figure		Page
19	Grain size gradient in the HAZ of 0.2% Cu-Al	55
20	Simulated grain growth kinetics, simulation matrix size: 500 × 500, random numbers: 1-100	56
21	Comparison of simulated grain size with real grain size in isothermally heated zone-refined tin	57
22	Simulated grain structure in zone-refined tin, heated at 185 C for (a) 75 sec, (b) 150 sec, (c) 225 sec, and (d) 300 sec, by GBM model	58
23	Comparison of simulated grain size with real grain size in a continuously heated Ti-alloy	59
24	Simulated β grain structures in a continuously heated Ti-alloy	60
25	Simulated grain growth kinetics, simulation matrix size: 800 × 600, random numbers: 1-10,000	61
26	The simulation time in the HAZ of 0.2% Cu-Al	62
27	Simulated and real grain structures in the HAZ of 0.2% Cu-Al alloy	63
28	Real grain size and simulated grain size in the HAZ of 0.2% Cu-Al alloy	64
29	Grain structure evolutions in the simulation, $f = 0.01$, initial location of the second phase particles: (a)-(e) only on grain boundaries; (f)-(j) randomly in the simulation matrix	65
30	Effect of size and initial location of second phase particles on grain growth kinetics, $f = 0.01$	66
31	Grain growth kinetics with 1-cell-sized second phase particles, initially located randomly in the simulation matrix	67
32	Relationship between D/r and f	68
33	Change in degree of contact during simulation, 1-cell-sized particles	69
34	Simulated grain growth kinetics with different N, the number of random orientation numbers	76

LIST OF FIGURES (Continued)

Figure		Page
35	The retarding force of a second phase particle on grain boundaries	77
36	Relationship between D/r and Rf	78
37	Degree of contact versus area fraction of second phase particles	79

INTRODUCTION

Grain Growth Kinetics

Grain growth is a process in which the mean grain size increases by consumption of grain boundary energy. In most engineering materials, grain size is an important microstructural feature. It contributes to the strength, ductility, toughness, corrosion resistance, heat resistance, phase transformation kinetics, and other properties of materials. Because of its importance, grain growth has been a topic of much research in materials science and engineering for many decades. In an overview paper, Atkinson[1] summarized the theories of grain growth in pure single phase systems. Although the understanding of the nature of grain growth has been greatly improved, there are still many interesting directions for research.

Empirical grain growth kinetics. The earliest grain growth kinetics was proposed by Beck et al. in 1947[2]:

$$D = C_1 t^n \tag{1}$$

where D was grain size, C_1 was a constant, t was time, and n was the time exponent. It is an empirical expression for isothermal grain growth.

Parabolic grain growth kinetics. Burke and Turnbull[3] derived a parabolic law for isothermal grain growth. They considered the migration of a grain boundary as the result of atom transport across the grain boundary under a pressure due to grain boundary curvature. Under this pressure, the grain boundary tends to migrate toward its center of curvature,

resulting in a reduction in total grain boundary area, hence total grain boundary energy. Their isothermal grain growth kinetics was expressed as

$$D^2 - D_o^2 = C_2 \exp(-\frac{Q}{RT})t \qquad (2)$$

where D_0 was initial grain size at $t = 0$, C_2 was a constant, Q was the activation energy for grain growth, R was the gas constant, and T was the temperature. In the derivation, they made the following assumptions:

1) the grain boundary energy was isotropic and independent of grain size;
2) the effect of inclusions in retarding grain growth was independent of temperature and grain size;
3) $r \propto D$, where r was the radius of grain boundary curvature and D was the mean diameter of grains;
4) $dD/dt \propto v$, where t was the time and v was the rate of grain boundary migration;
5) the grain boundary migration rate was proportional to driving force of grain growth:

$$v = MP \qquad (3)$$

where M was the grain boundary mobility and P was the pressure across the grain boundary, or the driving force of grain growth. P could be expressed as

$$P = \gamma(\frac{1}{r_1} + \frac{1}{r_2}) \qquad (4)$$

where γ was the grain boundary free energy and r_1 and r_2 were the principal radii of curvature of the grain boundary. For a spherical grain boundary, $r_1 = r_2 = r$.

Power law of grain growth kinetics. If it was assumed that the rate of grain boundary migration was proportional to $(\Delta F)^m$, i.e.,

$$v = M(\Delta F)^m \qquad (5)$$

where M was the grain boundary mobility and ΔF was the driving force of grain growth, a more common expression for grain growth kinetics was derived as

$$D^{\frac{1}{n}} - D_o^{\frac{1}{n}} = C_3 \exp(-\frac{Q}{RT})t \qquad (6)$$

where D_o was the initial grain size.

When $D_o << D$, Equation (6) will be simplified to Equation (1).

Topological analysis of grain growth. In a topological analysis of grain growth, Smith[4] emphasized that normal grain growth resulted from the interaction between the topological requirements of space-filling and the geometrical needs of surface tension equilibrium.

In a 2-D system, the structure consists of vertices joined by edges which surround faces. Provided the faces at infinity are not counted, the vertices, edges, and faces of any cellular structure obey the Euler's equation:

$$V - E + F = 1 \qquad (7)$$

where V, E, and F is the number of vertices, edges, and faces, respectively.

The number of edges joined to a given vertex is its coordination number z. For a topological stable structure, i.e., that in which the topological properties are unchanged by small deformations, z = 3 everywhere (z = 4 in a 3-D system), and the average number of edges, < n >, surrounding a face is 6. If a 4-rayed vertex occurs, it will be unstable and tend to decompose into two 3-rayed vertices as shown in Fig. 1.

Grain growth in a 2-D system is inevitable unless a structure consists of an absolutely regular array of hexagons, or grains. If one 5-sided grain is introduced into an array (and it has to be balanced by a 7-sided grain to maintain <n> = 6), then the sides of the grains must

become curved to maintain 120° angles at the vertices as shown in Fig. 2[5]. Grain boundary migration then tends to occur because of the curvature in order to reduce grain boundary area. Any grains with $n > 6$ will tend to grow because its boundaries are concave. Grains with $n < 6$ will tend to shrink because they have convex sides. Similar analysis was applied to grain structure evolution in 3-D systems.

Smith was the first to recognize the importance of topological space-filling requirements in grain growth. However, his analysis did not show the rate of the topological transformations and the overall grain growth. In contrast, Burke and Turnbull's parabolic law predicted the grain growth kinetics of spherical grains but did not attempt to find how the grains fill the space.

Rhines and Craig[6] pointed out that the volume (in 3-D) of the shrinking grain must be shared with grains throughout the system. Similarly, changes in topological parameters, the number of edges, faces, and vertices of grains, must also be propagated to every grain. The grain boundaries in the whole system must migrate for these propagation processes to occur. Rhines and Craig described this as grain boundary sweeping and defined a sweeping constant, θ, as the number of grains lost when grain boundaries throughout the system sweep through the equivalent of unit volume of material. Doherty[7] modified this definition of θ to θ^*, the number of grains which vanish when boundaries sweep through a volume equal to that of mean grain volume. Rhines and Craig[6] also introduced a concept of structural gradient, σ. They found σ to be approximately constant where σ was defined as

$$\sigma = \frac{M_V S_V}{N_V} \tag{8}$$

where M_V was the curvature per unit volume defined by

$$M_V = \int_{S_V} \frac{1}{2}\left(\frac{1}{r_1} + \frac{1}{r_2}\right) dS_V \tag{9}$$

and N_V was the number of grains per unit volume, S_V was the surface area per unit volume, and r_1 and r_2 were the principal radii of curvature. σ was a measure of the structural gradient in the system, i.e., the tendency to grain growth. Doherty[7] defined the mean curvature per grain, α, as the "structural gradient" in the system representing the tendency to grain growth:

$$\alpha = \frac{M_V}{N_V}. \tag{10}$$

Rhines and Craig derived, and this was later modified by Doherty by using the sweep constant θ^* instead of θ, the grain growth kinetics as

$$\bar{V} = \frac{\theta^* \mu \gamma M_V}{N_V} t + \bar{V}_0 \tag{11}$$

where $\bar{V}$ was the mean grain volume, μ was the grain boundary mobility, γ was the grain boundary energy, and $\bar{V}_0$ was the mean grain volume at time $t = 0$. Since θ^*, μ, γ, and M_V/N_V were approximately constant, $\bar{V}$ was proportional to t. Therefore, n, the time exponent of grain growth kinetics, was 1/3. This was different from the parabolic kinetics.

Mean field theories. The mean-field theories were initially developed by Feltham[8], Hillert[5], and Louat[9]. It dealt with the size change of an isolated grain embedded in an environment which represented the average effect of the whole array of grains. In these theories, there was an increase in the mean grain size and a decrease in the number of grains in the system during grain growth. This process was considered as a change of grain size distribution f(R) with time. It was seen in Fig. 3 that the grains with a given size R changed their size as the result of the following factors:

1) a diffusion-like process in which grains larger than $\bar{R}$ would grow due to the "concentration gradient" df/dR. However, the physical basis of the diffusion-like process was not clear.

2) a velocity v = dR/dt, due to a driving force associated with grain growth (assumed to be reduction in grain boundary curvature), so that grains were entering and leaving the size class R_2 along the time axis.

The overall flux of grains, j, was given by

$$j = -D\frac{\partial f}{\partial R} + fv \tag{12}$$

where D could be identified with a diffusion coefficient which only depended on the specific grain boundary mobility and f was the distribution function which was a function of both R and t. The continuity of the flux was

$$\frac{\partial f}{\partial t} = \frac{\partial}{\partial R}(-j) = \frac{\partial}{\partial R}(D\frac{\partial f}{\partial R}) - \frac{\partial}{\partial R}(fv). \tag{13}$$

The mean field theories of Feltham, Hillert and Louat all gave parabolic grain growth kinetics. These theories were essentially statistical and did not consider any topological constraints.

Grain growth as dislocation climb. A description of grain growth as dislocation climb was presented by Hillert (2-D)[5]. This was based on the introduction of a defect into a regular hexagonal 2-D array, as in Fig. 2. The defect pair of 5-7 sided grains moves stepwise through the array of grains as grain grows. For each growth step, the number of grains is decreased by one. The rate of grain growth depends on a combination of the number of defects per grain and the length of time a defect will take to make a grain shrink from average size to zero. Cahn and Padawer[10] identified the movement of Hillert's 5-7 defects

in the cell structure as equivalent to dislocation climb. Morral and Ashby[11] developed a 3-D version of Hillert's model. Parabolic grain growth kinetics were derived from such models.

Experimental Results on Grain Growth Kinetics

There are many reported experiments on isothermal grain growth in various metals and alloys in the literature. As can be seen in Table 1, most experimental results showed deviation of the time exponent n from the ideal value 0.5[12-20]. Some experiments showed a temperature dependence of the time exponent n[21-25]. Fig. 4 shows the relationship between the time exponent and normalized annealing temperature[2, 12-14, 16, 17, 21-23, 26-29]. The failure of the experimental data to conform to the parabolic law, i.e., Equation (2), has been attributed to a number of material related factors:

Table 1. Experimental results of time exponent in grain growth kinetics

Material	Temperature range, K	Time exponent n	Reference
Zone-refined tin	440-493	0.50	[12]
Zone-refined lead	441-591	0.40	[13]
Zone-refined aluminum	351-486	0.24	[14]
Zone-refined Al+400 at.ppm Cu	545-680	0.31	[14]
α-brass	723-973	0.21	[15]
Titanium	673-873	0.33	[16]
Zirconium	773-873	0.35	[17]
Cadmium	513-518	0.5	[18]
Cadmium-0.01%at Ag	548-573	0.5	[18]
Zone-refined tin	443-473	0.43	[19]
Zone-refined lead	483-573	0.41	[19]
Al-Mg alloy	550-800	0.5	[20]

1) grain growth is in a transient period[30, 31];

2) pinning forces from second phase particles[32];

3) pinning forces from the specimen thickness effect[21, 33];

4) intrinsic drag forces on grain boundaries[34];

5) solute drag effect[35];

6) onset of abnormal grain growth[36, 37];

7) neglect of initial grain size effect[33, 38].

Zener Pinning

Zener pinning refers to the inhibiting effect of second phase particles on grain growth in polycrystalline materials. Zener[39] proposed an analytical model for such pinning on grain growth:

$$\frac{\rho}{r} = \frac{4}{3} f^{-1} \tag{14}$$

where ρ was the net curvature radius of the grain boundary, r was the mean radius of second phase particles, and f was the volume fraction of second phase in the material. This model has been described in many textbooks[40-42]. In application of the Zener model to the limitation of grain growth in the presence of second phase particles, the radius of curvature is usually taken as mean grain size. However, the prediction of the grain size limit by Zener's model typically deviates significantly from experimental results. The exponent of the f term in real materials is usually different from -1. Hellman and Hillert[43] introduced a correction factor β based on a "dimple model." They also suggested that the curvature radius of the grain boundary was 3 times the grain size, i.e., $\rho = 3D$. Their modified model was

$$\frac{D}{r} = \frac{8}{9} (\beta f)^{-1} \tag{15}$$

where D was the grain size of the pinned structure. The correction factor β in their model was a weak function of D/r and decreased if the volume fraction of second phase increased to a high level. Hillert[44] found that the correction factor β was proportional to $f^{-0.07}$ in the ρ/r range of 9 to 10,000, and rewrote Equation (15) as

$$\frac{D}{r} = \frac{8}{9} f^{-0.93}. \tag{16}$$

In Monte Carlo simulation of grain growth in the presence of second phase particles in a 2-D system, Srolovitz et al.[45] obtained a different relationship between pinned grain size and the second phase particle size:

$$\frac{D}{r} = 3.4 f^{-0.5}. \tag{17}$$

The simulation results of Doherty et al.[46] confirmed the results. Anderson et al.[47] obtained an $f^{-1/3}$ relation from 3-D computer simulation:

$$\frac{D}{r} = 1.8 f^{-0.33}. \tag{18}$$

In all of the above models, there was an assumption of randomly distributed second phase particles throughout the alloy systems. However, if the second phase particles tend to prohibit grain growth by pinning grain boundaries, it should be expected that the particles would accumulate on grain boundaries. Such an accumulation would make the location of second phase particles not random but preferred at boundaries. It can be expected that the apparent volume fraction of the particles on grain boundaries, i.e., the volume fraction that the grain boundary experiences, should be greater than that in the whole of the material. Therefore, it is more reasonable to replace the volume fraction of second phase in the material by the apparent volume fraction of second phase on grain boundaries.

Liu and Patterson[48,49] examined the interaction between pores and grain boundaries in sintering. They introduced a degree of contact beyond random between grain boundaries and pores to treat their interaction and obtained the relationship:

$$\frac{\rho}{r} = \frac{4}{3}(Rf)^{-1} \tag{19}$$

where R was the degree of contact between grain boundaries and pores. The R was defined as the ratio of the measured length of triple line of intersection between grain boundaries and pore surfaces to the length expected to exist from random intersections between grain boundaries and pore surfaces. For random intersections, R = 1. If pores accumulate preferentially on grain boundaries, R > 1. This analysis is also applicable to the interaction between grain boundaries and second phase particles, and most of the above models have recently been reanalyzed employing the R term[50].

Monte Carlo Simulation Technique

Anderson et al.[51] presented a computer simulation technique to observe grain growth, namely Monte Carlo simulation. The Monte Carlo simulation technique has been applied to the simulation of normal grain growth[52-54], abnormal grain growth[55,56], Zener pinning of second phase particles in grain growth[47,57,58], grain growth in the heat affected zone (HAZ) of welds[59], recrystallization[60,61], and castings[13,62,63].

A detailed description of Monte Carlo simulation procedures can be found in Anderson et al.[51]. In Monte Carlo simulation, the microstructure was mapped onto a discrete lattice. The lattice could be triangular, square, or any shape. However, a lattice with triangular arrangement, as shown in Fig. 5, was often used. Each lattice site was assigned a random number S_r, $1 \leq S_r \leq N$. When N was small, grains of the same orientation

impinged frequently. The assigned random number S_r was referred to as the lattice site orientation number representing the orientation of the grain in which it was embedded. A cluster of adjacent lattice sites with the same orientation number was considered as one grain. Grain boundaries existed between two adjacent sites with different orientation numbers.

A lattice site was selected at random, and a new trial orientation number was also chosen at random from the other (N - 1) possible orientations. The probability that a lattice site changes its orientation number was determined by evaluating the energy change ΔE when switching the orientation number at a lattice site from S_o to S_n where ΔE was calculated by

$$\Delta E = J \cdot \Sigma(\delta_{S_i S_o} - \delta_{S_i S_n}) \tag{20}$$

where S_o was the original orientation number at a lattice site, S_i were the orientation numbers of its six nearest neighbors, S_n was a new random orientation number, J was the interaction energy, and δ was the Kronecker function. The summation went over all six of the nearest neighbor sites. The successful reorientation probability was calculated by

$$P = \begin{cases} \exp(-\dfrac{\Delta E}{kT}) & (\Delta E > 0) \\ 1 & (\Delta E \le 0). \end{cases} \tag{21}$$

If $0 < P < 1$, P was compared to a new random number P_c which fell between 0 and 1. When $P \ge P_c$, then the reorientation attempt was successful; otherwise, no reorientation occurred.

If the energy change ΔE, as described in Equation (20), was much greater than kT, or if $T = 0$ was assumed, then $\exp(-\Delta E/kT) \doteq 0$, and Equation (21) was simplified as

$$P = \begin{cases} 0 & (\Delta E > 0) \\ 1 & (\Delta E \le 0). \end{cases} \tag{22}$$

Almost all Monte Carlo simulations of grain growth in the literature assumed $T = 0$.

After all lattice sites experience one reorientation attempt, the simulation completed one Monte Carlo simulation step, or one iteration of the Monte Carlo simulation. A Monte Carlo simulation step was also referred to as the Monte Carlo simulation time.

The driving force of grain growth in Monte Carlo simulation was the reduction of grain boundary area, hence the reduction of grain boundary energy in the system. The mean curvature, k, for each individual grain was found to be (for 2-D)

$$k = \frac{\pi(n-6)}{3S} \tag{23}$$

where S was the grain perimeter.

Anderson et al.[51] found that the grain growth exponent (n) in Monte Carlo simulation was a function of N. They also found that the prefactor k was inversely proportional to $\sqrt{N}$. It should be noted that, in their analysis of n, the simulation time was assumed to be proportional to real time.

Radhakrishnan and Zacharia[52] modified the Monte Carlo simulation by selecting the new trial orientation number at random from the nearest neighbors' orientations instead of from the other (N - 1) possible orientations. This accelerates the simulation process.

To simulate grain growth in real material systems, the conversion of simulation time to real time is essential. Ling and Anderson[64] pointed out that the conversion of MC simulation time to real time required an implicit activation energy factor [exp(-W/kT)], which corresponded to the atomic jump frequency. By comparing the results from the soap froth experiment and Monte Carlo simulation, Ling et al.[65] related the Monte Carlo simulation time (t_{MC}) to real time (t_r) by $t_r(\text{min}) = 0.32 t_{MC} + 2044$. Radhakrishnan and Zacharia[66] related Monte Carlo simulation time to real time-temperature by $MCS = K_1 K_2^0 \exp(-\frac{Q_M}{RT})t$, where

MCS was Monte Carlo simulation time, K_1 and K_2^0 were constants, Q_M was the activation energy for grain boundary migration, R was the gas constant, T was temperature, and t was real time. Thompson and Liu[67], Shen[68] and Shen et al.[69] connected simulation time to real time and real temperature by $MCS = \nu \exp(-\frac{Q}{RT})t$, where ν was the atomic vibration frequency, Q was the activation energy, and R was the gas constant. In all models above, the Monte Carlo simulation time was related linearly to the real time. Gao and Thompson[53] presented two different models that connect the real time-temperature to simulation time. These are presented in the Monte Carlo Simulations section of Experimental Procedures.

Thermal Field in HAZ

Rosenthal[70] derived equations to describe heat flow in 3-, 2.5-, and 2-D situations which correspond to the welding of thick, fairly thick, and thin plates:

$$for\ 3\text{-}D \qquad T - T_0 = \frac{\Phi}{2\pi k}\exp(-\lambda \nu \xi)\frac{\exp(-\lambda \nu R)}{R} \tag{24}$$

$$for\ 2.5\text{-}D \qquad T - T_0 = \frac{\Phi \lambda \nu}{2\pi k}\exp(-\lambda \nu \xi)\sum_{n=-\infty}^{\infty}\frac{\exp(-\lambda \nu R_n)}{R_n} \tag{25}$$

$$for\ 2\text{-}D \qquad T - T_0 = \frac{\Phi}{2\pi kg}\exp(-\lambda \nu \xi)K_0(-\lambda \nu R) \tag{26}$$

where T was the instantaneous temperature in K, T_0 was the initial temperature in K, g was the plate thickness, k was the thermal conductivity, K_0 was a Bessel function of the first kind zero order, λ was half reciprocal of thermal diffusivity ($\lambda = 1/(2\alpha_s)$), ξ = x-vt where t was time ($\nu < 0$), Φ was the arc power, and $R = \sqrt{\xi^2 + y^2 + z^2}$.

The above solutions to the differential equation of heat flow were derived under the following assumptions:

1) the electrode was not heated by the Joule effect;

2) the plate was isotropic, homogeneous, single phase at all times, and infinite except when dimensions were quoted;

3) the heat was supplied from a point source for 3-D and 2.5-D and a vertical line source for 2-D heat flow;

4) thermal conductivity and diffusivity were invariant with temperature; and

5) the latent heat of fusion and heat losses from the plate were negligible.

Christensen et al.[71] and Hess et al.[72] showed that Equations (26) and (24) accurately predict isothermal widths and cooling rates for 2-D and 3-D heat flow situations for a wide range of welding conditions. The arc power in the welding processes could be calculated by

$$\Phi = \eta VI \tag{27}$$

where V and I were the welding voltage and current, and η was the arc efficiency, which depended on the welding process.

In recent years, the finite difference and finite element methods (FEM) were widely used in the calculation of heat flow problems. There are several commercial versions of FEM software available.

Models for Grain Growth in the HAZ

Ashby-Easterling's model[73]. In this model, thermal cycles in the HAZ of welds were given by the equations of Rosenthal[70,74].

For thick plates, the equation was

$$T - T_0 = \theta_1 \frac{\Delta t}{t} \exp\left[-\frac{\Delta t}{et}\left(\frac{\theta_1}{T_p - T_0}\right)\right] \tag{28}$$

where $\frac{1}{\theta_1} = \left(\frac{1}{773 - T_0} - \frac{1}{1073 - T_0}\right)$, T_0 was the preheat temperature, T_p was the peak temperature, and Δt was the time to cool from 800 C to 500 C.

For thin plates, the thermal cycles were expressed as

$$T-T_0 = \theta_2(\frac{\Delta t}{t})^2 \exp[-\frac{\Delta t}{2et}\frac{\theta_2^2}{(T_p-T_0)^2}] \quad (29)$$

where $\frac{1}{\theta_2^2} = [\frac{1}{(773-T_0)^2} - \frac{1}{(1073-T_0)^2}]$.

The grain growth rate was given by

$$\frac{d\phi}{dt} = Af(\phi)\exp[-\frac{Q}{RT(t)}] \quad (30)$$

where ϕ was the grain size, A was a constant, $f(\phi)$ was a function of ϕ, Q was the activation energy, R was the gas constant, and T(t) was the temperature. Integration over the thermal cycle yielded

$$\int_{\phi_i}^{\phi_f}\frac{d\phi}{Af(\phi)} = \int_0^{\tau}\exp[-\frac{Q}{RT(t)}]dt \quad (31)$$

where ϕ_i and ϕ_f were initial and final grain size, respectively. The left hand side of Equation (31) was a constant for a fixed change in grain size ϕ.

Suppose that the mean grain sizes, ϕ_1, at points in the HAZ were known. The thermal cycles at each of these points could be calculated from either Equation (28) or (29) based on T_p and Δt at these points. Assuming an activation energy and applying the thermal cycles to the right hand side of Equation (31) yielded

$$\int_0^{\tau}\exp[-\frac{Q}{RT(t)}]dt = I. \quad (32)$$

A contour in the T_p-Δt plot, corresponding to the mean grain size ϕ_1, was drawn by choosing other pairs of T_p and Δt, calculating the thermal cycle, and integrating Equation (32) to get Γ. If Γ was not close enough to I (within 5%), Δt was adjusted and a new attempt was made. If the above contour did not fit the rest of the grain size data, the activation energy, Q, was

adjusted and the entire procedure repeated until the contour fitted the rest of the grain size data. This procedure was repeated for other I values to obtain other contours corresponding to grain size ϕ_n (n = 2,3,4...).

When second phase particles are in the metallurgical system, the grain boundaries will be pinned by these particles. The grain growth law should be written as

$$\frac{d\phi}{dt} = A[f(\phi) - P(T(t))]\exp[-\frac{Q}{RT(t)}] \tag{33}$$

where P is a pinning force which is a function of temperature.

When the pinning force P remains large until the second phase particles dissolve completely at temperature T_s (as shown below) and then falls instantaneously to zero, Equation (32) is still valid, with the limits of integration changed to meet this condition. The dissolution temperature T_s can be calculated from the equilibrium solubility product of the second phase. For example, the equilibrium solubility product for the reaction of

$$aM + bC = M_aC_b \tag{34}$$

was given by

$$\log(C_M^a C_C^b) = A - \frac{B}{T}. \tag{35}$$

The dissolution temperature of the carbide, T_s, could be expressed as

$$T_s = \frac{B}{A\log(\frac{C_M^a C_c^b}{f^{a+b}})}. \tag{36}$$

The results of this model gave a diagram for grain growth in the HAZ as shown in Fig. 6[73].

Alberry-Chew-Jones's model[75]. The grain growth kinetics of an alloy system of interest was obtained from the isothermal grain growth experiment. At a given temperature,

the grain size increased with time according to following expression (note m = 1/n, where m was the grain growth exponent, n was the time exponent):

$$D_1^m - D_2^m = K(t_1 - t_2) \tag{37}$$

where D_1 and D_2 were the grain size at time t_1 and t_2, respectively. The grain growth exponent m and the time constant K were evaluated by a series of least-squares plots of $(D_1^m - D_2^m)$ against $(t_1 - t_2)$. The K values from curve fitting of experimental data to Equation (37) at each temperature were related to temperature by

$$K = A\exp(-\frac{Q}{RT}). \tag{38}$$

By a plot of K against 1/T, the A and Q values were determined. Thus, the grain growth kinetics were given by

$$D_1^m - D_2^m = A\exp(-\frac{Q}{RT})(t_1 - t_2). \tag{39}$$

Application of Equation (39) to a non-isothermal process, assuming $D_2 = 0$, yielded

$$D^m = \sum A\exp(-\frac{Q}{RT})\Delta t. \tag{40}$$

Equation (40) was the start point of Alberry-Chew-Jones's model. In a 0.5Cr-Mo-V steel, Alberry et al. got the following equation:

$$D^{2.7} = \sum 1.41\times10^{13}\exp(-\frac{460{,}000}{RT})\Delta t. \tag{41}$$

However, Alberry et al. found that the predicted grain size was larger than real grain size when Equation (41) was applied to a real-weld HAZ of 0.5 Cr-Mo-V steel. In the prediction, they calculated the thermal cycles in the HAZ by Rosenthal's equations[71], i.e.,

$$T(t) = T_0 + \frac{q\eta}{2\pi k r}\exp(-\lambda v(r - vt)). \tag{42}$$

To fill the gap between the predicted grain size and the real grain size, they introduced a correction factor, the thermal pinning factor M, and rewrote Equation (40) as

$$D^{M} = \sum A \exp(-\frac{Q}{RT})\Delta t. \quad (43)$$

They found M = 0.47 For 0.5Cr-Mo-V steel and modified Equation (41) as

$$D^{1.30} = \sum 5.4\times10^{12} \exp(-\frac{460{,}000}{RT})\Delta t. \quad (44)$$

The prediction of grain size by Equation (44) agreed much better with the grain size in their real-weld HAZ, as shown in Fig. 7.

The Goals of the Present Work

1) Establish real time-temperature Monte Carlo simulation models for grain growth.
2) Apply the above models to grain growth in isothermal processes, continuous heating processes and the HAZ of welds.
3) Validate the simulation model by experimental results.

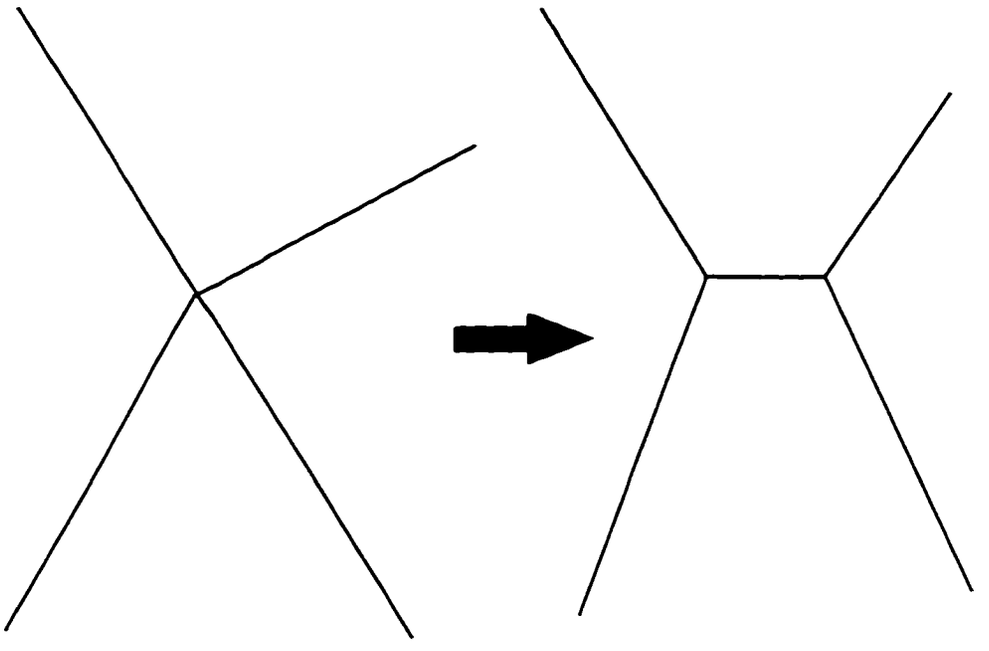

Fig. 1. The 4-rayed vertex tends to decompose to two 3-rayed vertices.

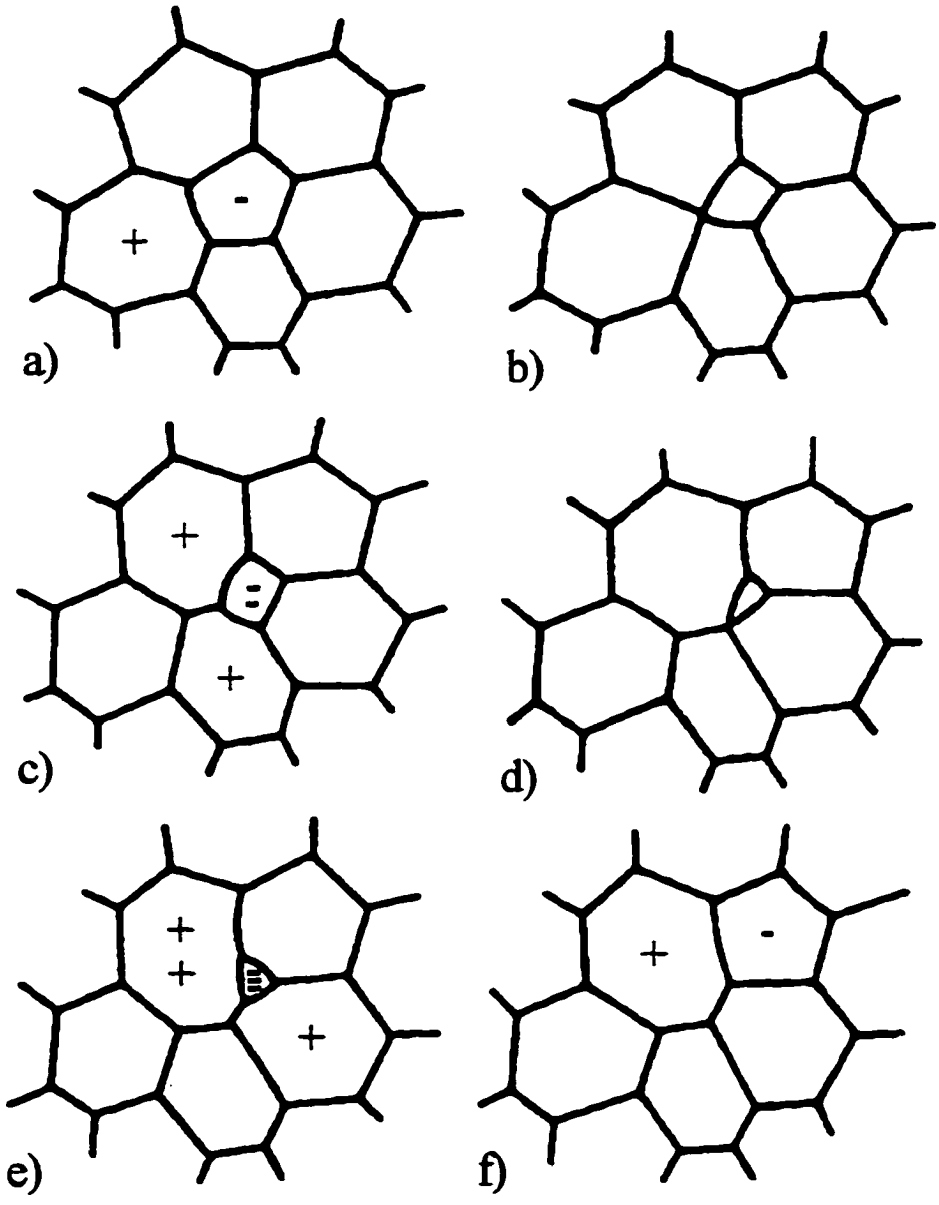

Fig. 2. 2-D grain structure evolution (after [5]).

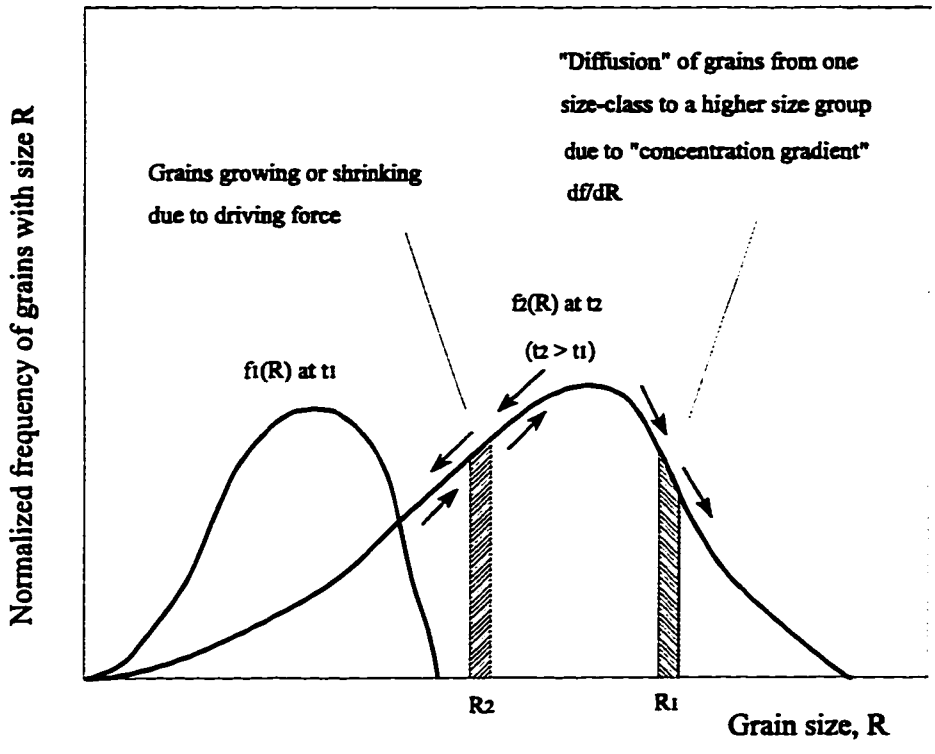

Fig. 3. Grain size distribution (after [1]).

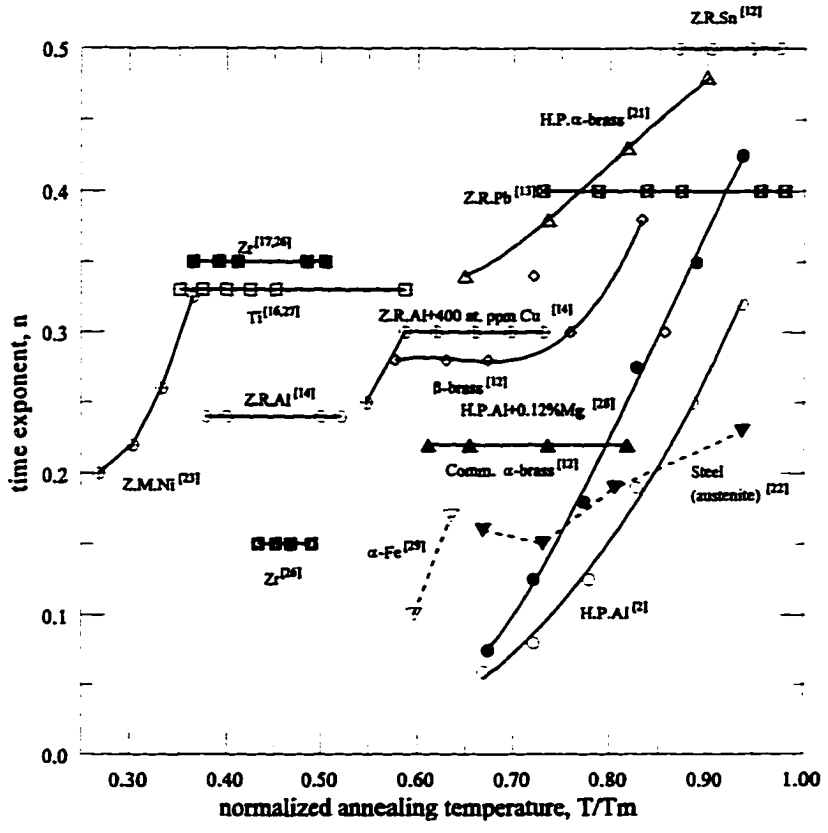

Fig. 4. Temperature dependence of the time exponent in isothermal grain growth.

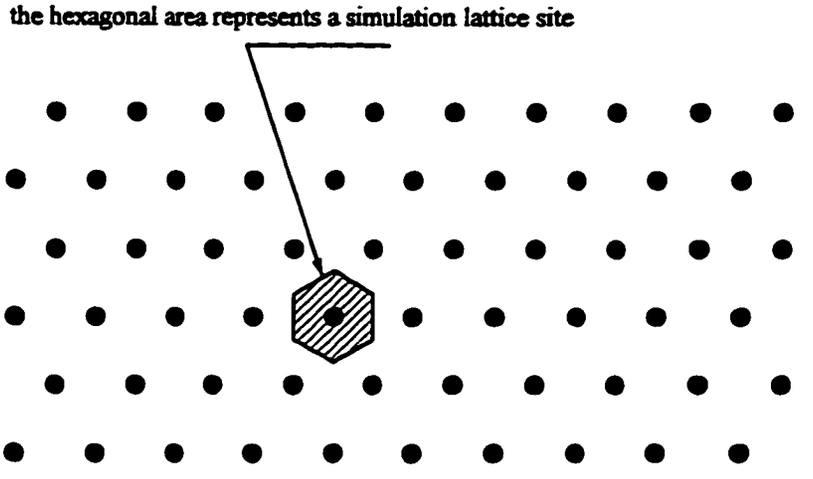

Fig. 5. Triangular simulation matrix.

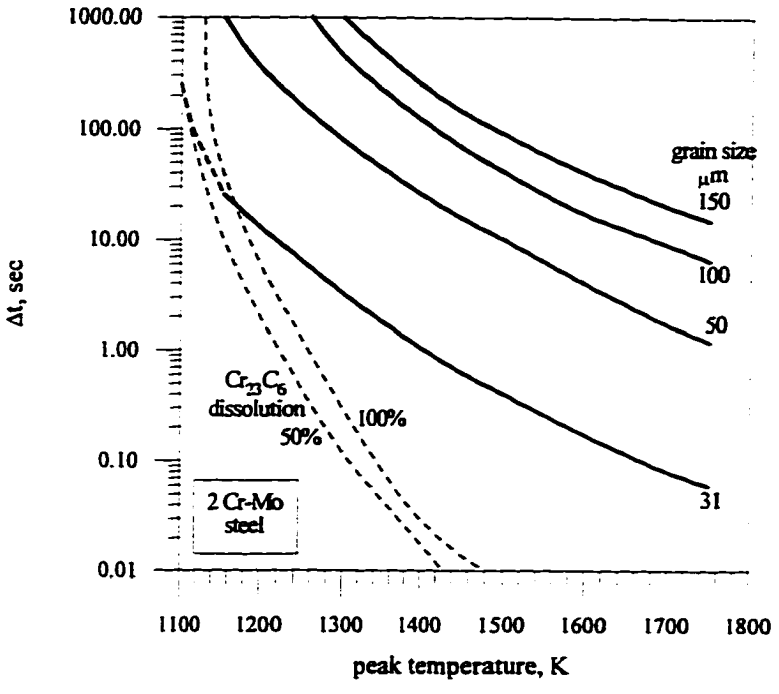

Fig. 6. A diagram for a 2% Cr-Mo steel, thick plate, T_0 = 300K (after [73]).

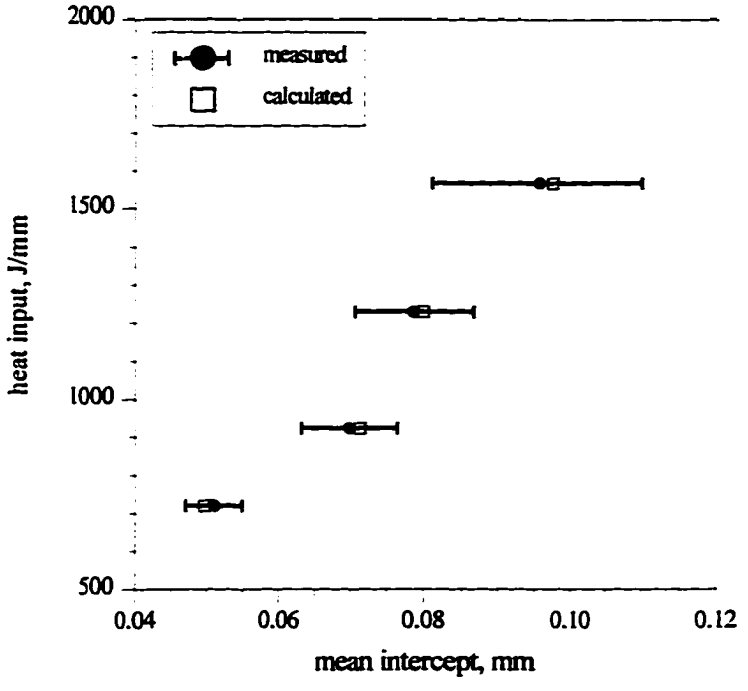

Fig. 7. Comparison of calculated grain size to experiment data (after [75]).

EXPERIMENTAL PROCEDURES

Sample Preparation

A laboratory melted Al-Cu alloy was produced by Alcoa. The metal was received in slabs measuring 150 × 75 × 20 mm. The chemical composition of the alloy is given in Table 2. These slabs were initially cut to 40 × 20 × 20 mm samples.

Table 2. Chemical compositions of the experimental alloy (wt%)

Cu	Si	Fe	Ti	B	Mn	Mg	Sn	Zn	Cr	Al
0.21	0.00	0.00	0.0003	0.0001	0.00	0.00	0.00	0.00	0.00	balance

The samples were cold rolled from 20 mm to 5 mm, producing a reduction of 75%. The cold rolled samples were divided into two groups. The first group of samples was cut into 12 × 6 × 5 mm samples and used in isothermal grain growth experiments. The second group was recrystallized at 300 C for 10 minutes, and then cut to 90 × 25 × 5 mm. The second group of samples was prepared for welding experiments.

Isothermal Grain Growth

In the isothermal grain growth experiments, the samples were suspended in a $NaNO_3$ salt pot at preset temperatures by a thin copper wire and held for a series of times, then quenched in water. Table 3 lists the schedule of the isothermal grain growth experiment.

Metallographic Sample Preparation

The samples were ground on SiC papers and polished using 1 μm alumina slurry. The samples were electrolytically etched in a solution of 4.6 ml 50% fluoboric acid + 0.7g boric

Table 3. Heat treatment for grain growth kinetics

Sample ID	Temperature (C)	Time (seconds)	Sample ID	Temperature (C)	Time (seconds)
201	540	60	215	500	600
202	540	30	221	450	30
203	540	120	222	450	60
204	540	10	223	450	120
205	540	300	224	450	300
206	540	600	225	450	600
211	500	60	231	400	300
212	500	120	232	400	120
213	500	30	233	400	600
214	500	300	234	400	3600

acid + 100 ml H_2O at 20 volts for 1-3 minutes. A polarized light microscope was used to observe the microstructures.

Welding Experiments

Figure 8 shows the experimental welding set-up. A model TIG-250 Lincoln ArcWelder was used as the power supply for the GTAW welding experiments. A 3 mm electrode was used. The arc travel speed was controlled at 7.5 inches per minute by the torch carriage. Eight pairs of 0.25 mm thermocouples were attached to the sample. The attachment was made by drilling a tiny hole, 1 mm in diameter, on the sample surface for each pair of thermocouples. The thermocouples were inserted into the holes, and the surrounding area was slightly deformed to secure the thermocouples. To ensure the proper spacing between the thermocouples, the thermocouples were not arranged in one straight line. Figure 9 shows

the arrangement of the thermocouples on the sample surface. Ceramic insulators and plastic sheaths were put on the thermocouples to electrically insulate the thermocouple wires.

The sample was clamped in a jig to secure it during welding. The gap between the electrode tip and the sample to be welded was 1 mm. During the welding experiment, the temperature in the sample was measured by a LabWindows data acquisition system using the embedded thermocouples. Using this set-up, eight channels of temperature data could be read essentially simultaneously by the LabWindows system. To achieve a steep thermal gradient in the 0.2% Cu-Al sample, a heat sink was attached to the bottom of the sample by putting the jig in water and submerging the lower part of the sample in water.

Grain Size Measurement

The grain size was measured by the mean intercepts of grains. A test line of length L_T was placed randomly on the microstructures. The number of intercepts between the test line and the grain boundaries P_T was counted. The mean intercept d was calculated by

$$d = \frac{L_T}{P_T} \tag{45}$$

In actual operation, a grid was put in the eyepiece of the microscope. The lines on the grid were used as test lines.

The standard error of the measurement was given by[76]

$$SE = \sqrt{\frac{\sum [(P_T)_i - \bar{P}_T]^2}{N(N-1)}} \tag{46}$$

where $(P_T)_i$ was the ith measurement of P_T, $\bar{P}_T$ the mean value of $(P_T)_i$, and N the total number of measurements. The 95% confidence intervals of the measurements were

$$95\%\ C.I. = \bar{P}_T \pm 2SE. \tag{47}$$

The test lines were put parallel to the fusion line to measure the grain size in the HAZ. The mean grain size at position x in the HAZ was the average of grain size measurements taken from locations with the same distance, x, from the fusion line. The mean grain size was plotted against the position x to describe the grain size gradient in the HAZ.

Calculation of the Degree of Contact Between Grain Boundaries and Second Phase Particles

The degree of contact between grain boundaries and second phase particles was defined as the ratio of area fraction of second phase particles on grain boundaries to that in the material. The area fraction of second phase particles on grain boundaries was taken as

$$f_{gb} = \frac{\pi r^2 (N_A^{\beta})_{gb}}{2r[L_A^{\alpha\alpha} + (L_A^{\alpha\alpha})_{missing}]} \tag{48}$$

where $(N_A^{\beta})_{gb}$ was the number of second phase particles touching grain boundaries per area, $L_A^{\alpha\alpha}$ was the length of grain boundaries per area, $(L_A^{\alpha\alpha})_{missing}$ was the length of "missing" grain boundaries per area (see Fig. 10), and r was the mean radius of particles.

Since

$$\begin{aligned} L_A^{\alpha\alpha} &= \frac{\pi}{2} P_L^{\alpha\alpha} \\ (L_A^{\alpha\alpha})_{missing} &= r P_A^{\alpha\alpha\beta} \end{aligned} \tag{49}$$

the R value was calculated as

$$R = \frac{\pi r (N_A^{\beta})_{gb}}{f(\pi P_L^{\alpha\alpha} + 2r P_A^{\alpha\alpha\beta})} \tag{50}$$

where $P_L^{\alpha\alpha}$ was the number of grain boundary intercepts with test lines per unit area and $P_A^{\alpha\alpha\beta}$ was the number of triple points where grain boundaries met particles per unit area, as shown in Fig. 10.

Monte Carlo Simulations

The Monte Carlo simulations were performed using a Pentium-120 PC and a Model 5/266 DEC AlphaStation. The simulation results were saved as ASCII files and input into Grapher to generate the microstructure of grains.

The basic procedures of the Monte Carlo simulation technique were described in Monte Carlo Simulation Technique section of Introduction. The critical step for the application of the Monte Carlo simulation technique to real metallurgical processes is the conversion of real temperature and real time into simulation time, i.e., the number of simulation iterations.

In the present work, two different models for converting the real temperature and real time to the simulation time were developed[53], namely the grain boundary migration (GBM) model and the experimental data based (EDB) model.

Grain boundary migration (GBM) model. In the simulation matrix, grain boundaries existed between two adjacent lattice sites with different orientation numbers. The reorientation of a lattice site could be taken as the migration of a grain boundary segment. The migration velocity (v) of grain boundaries was expressed as[40]

$$v = \frac{AZv V_m^2}{N_a RT} \exp\left(\frac{\Delta S_a}{R}\right) \exp\left(-\frac{Q}{RT}\right)\left(\frac{2\gamma}{r}\right) \qquad (51)$$

where A was the accommodation probability, Z was the average number of atoms per unit area at the grain boundary which could be taken as the weighted average number of atoms on close packed crystalline planes, v was the atomic vibration frequency, N_a was the Avogadro's number, R was the gas constant, T was the absolute temperature, ΔS_a was the

activation entropy, Q was the activation energy, γ was the grain boundary energy, and r was the grain boundary curvature radius. Assuming that

1) The grain boundary curvature radius r was equal to the mean grain intercept[3].
2) The velocity of grain boundary migration was associated with the growth rate of the mean grain intercept by $v = \frac{dr}{dt} = \frac{dL}{dt}$, where L was the mean intercept of grains.
3) The activation entropy of grain boundary migration, ΔS_a, was equal to the fusion entropy of the material, ΔS_f, due to similarity between the structure of grain boundaries and that of a liquid.
4) Grain boundary energy, γ, was independent of grain size and grain orientation.
5) The atomic vibration frequency, v, was related to temperature as[3] $v = \frac{kT}{h} = \frac{RT}{N_a h}$, where h was Planck's constant, and k was Boltzmann's constant.

Equation (51) was rewritten as

$$LdL = \frac{2\gamma AZV_m^2}{N_a^2 h}\exp(\frac{\Delta S_f}{R})\exp(-\frac{Q}{RT})dt. \quad (52)$$

Integrating Equation (52) yielded

$$L^2 - L_o^2 = \frac{4\gamma AZV_m^2}{N_a^2 h}\exp(\frac{\Delta S_f}{R})\exp(-\frac{Q}{RT})t \quad (53)$$

where L_0 was the initial grain size at t = 0.

A simulated grain growth kinetics was defined as the relationship between the simulated grain size and the number of simulation iterations needed to generate a specific grain size. The simulated grain growth kinetics took the following form by regression analysis of the data generated from Monte Carlo simulation:

$$L = K_1 \lambda (MCS)^{n_1} \quad (54)$$

where L was the simulated mean grain intercepts, K_1 and n_1 were model constants, λ was thelattice point spacing, and MCS was the number of Monte Carlo simulation iterations.

Equating the mean grain intercept of Equation (53) and that of Equation (54) yielded

$$(MCS)^{2n_1} = (\frac{L_o}{K_1\lambda})^2 \cdot \frac{4\gamma AZV_m^2}{N_a^2 h K_1^2 \lambda^2} \exp(\frac{\Delta S_f}{R}) \exp(-\frac{Q}{RT}) t. \quad (55)$$

To apply Equation (55) to grain growth simulation during continuous heating and/or cooling processes, the grain growth time, t, had to be divided into a series of small time intervals t_i (i = 1,2,...,x) and Equation (55) was rewritten as

$$(MCS)^{2n} = (\frac{L_o}{K_1\lambda})^2 \cdot \frac{4\gamma AZV_m^2}{N_a^2 h K_1^2 \lambda^2} \exp(\frac{\Delta S_f}{R}) \Sigma [\exp(-\frac{Q}{RT_i}) t_i] \quad (56)$$

where the summation went from i = 1 to i = x, and T_i was the temperature in time interval t_i.

Equations (55) and (56) were the relationships used for real time-temperature simulation in the GBM model.

Experimental data based (EDB) model. Using multiple regression analysis of experimental grain growth data, a relationship between grain size (L), holding time (t) and temperature (T) was obtained:

$$L^n - L_0^n = K_0 \exp(-\frac{Q}{RT}) t. \quad (57)$$

Substituting Equation (54) into Equation (57) gave a relationship between the Monte Carlo simulation time associated with isothermal grain growth and real time and temperature:

$$(MCS)^{nn_1} = (\frac{L_0}{K_1\lambda})^n \cdot \frac{K_0}{(K_1\lambda)^n} \exp(-\frac{Q}{RT}) t. \quad (58)$$

Equation (58) could be applied directly to isothermal processes, but it must be integrated over the entire thermal cycle for applications to continuous heating and/or cooling processes. This could be done by summing the grain growth in short time intervals at different temperatures, i.e.,

$$(MCS)^{n_{n-1}} = \left(\frac{L_0}{K_1\lambda}\right)^n + \frac{K_0}{(K_1\lambda)^n}\sum \left[\exp\left(-\frac{Q}{RT_i}\right)t_i\right] \qquad (59)$$

where T_i was the temperature in time interval t_i.

Equations (58) and (59) were the relationships between the number of Monte Carlo simulation iterations and real time-temperature for the EDB model.

Monte Carlo simulation of Zener pinning. The Monte Carlo simulations of grain growth can be applied to both systems that do not have any second phase particles and systems that contain second phase particles. One important phenomenon in grain growth of a system with second phase particles is Zener pinning. Zener pinning of grain growth was simulated in 500 × 500 2-D triangular matrices. The orientation numbers of lattice sites ranged from 1 to 100. A special negative orientation number, -20, was assigned to the lattice sites where the second phase particles were embedded. Figure 11 shows the configuration of second phase particles in the simulation matrix. The particles in the simulations were 1, 2, or 3 cell sized. The particle area fractions ranged between 0.001 and 0.15. In each run of the simulations, the second phase particles were immobile and monosized. There was neither growth nor dissolution of the second phase particles. A modified Monte Carlo simulation algorithm was applied in the simulations[52]. The switching probability from one orientation number to another was also given by Equation (21). The switching of the orientation number

of second phase particles was totally prohibited, which inferred that the second phase particles were immobile.

The initial simulation matrix was produced by running Monte Carlo simulation without second phase particles until the mean grain intercept reached 5λ, where λ was the lattice site spacing. The simulations started by planting the monosized second phase particles into the base simulation matrix. Two initial locations of the second phase particles were selected: (a) all second phase particles located only on grain boundaries of the base matrix, and (b) all second phase particles located randomly in the base matrix. The grain growth simulation was performed until the mean grain size stopped increasing, that is, until the grain structure was pinned. The mean grain intercept and degree of contact between grain boundaries and second phase particles were recorded during the simulations.

Monte Carlo simulation of grain growth in the weld HAZ. The EDB model was used in the simulation of grain growth in the weld HAZ. The thermal cycles measured during the welding experiments using LabWindows were coupled into Equation (59) to generate the required simulation time for the grain growth simulation in the HAZ. Since the difference in grain growth might be quite significant at different peak temperatures in the HAZ, half periodic boundaries were used, i.e., only the matrix boundaries parallel to the thermal gradient were wrapped.

A: torch carriage B: heat sink C: torch D: sample

E: power source F: thermocouples G: LabWindows data acquisition system

Fig. 8. Experimental welding set-up.

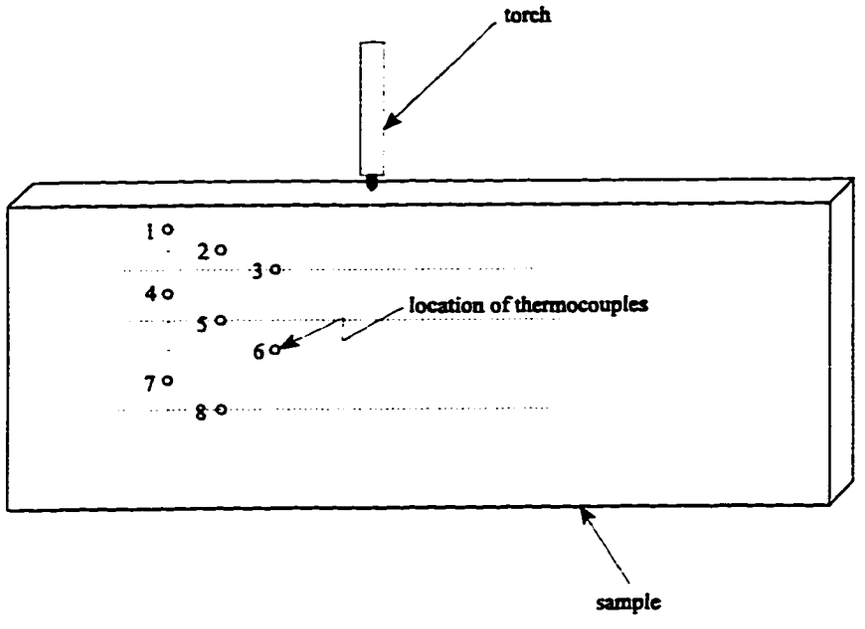

Fig. 9. The locations of thermocouples on the sample surface.

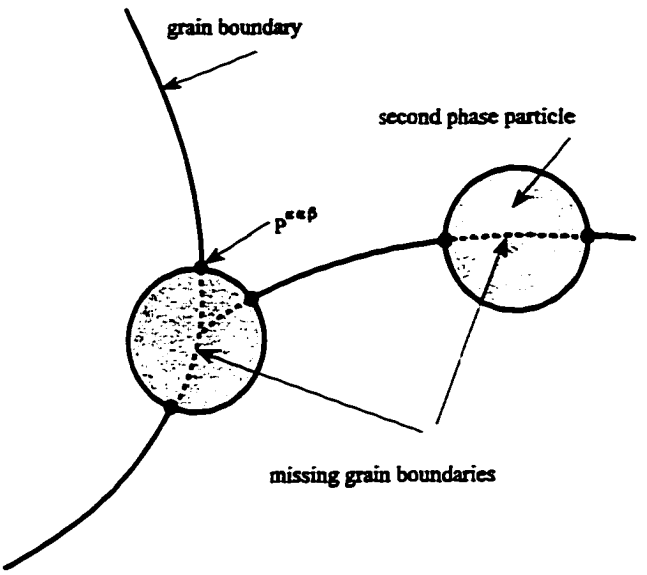

Fig. 10. Intersection of second phase particles and grain boundaries.

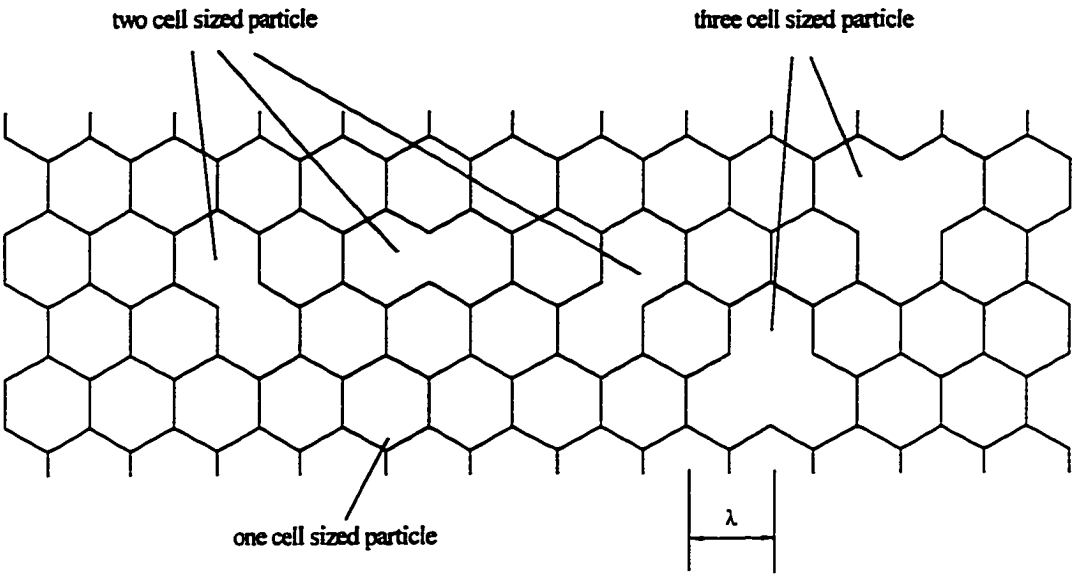

Fig. 11. Configuration of second phase particles in the simulation matrix.

EXPERIMENTAL RESULTS

Grain Growth Kinetics

The grain growth kinetics in the material of interest is required for the application of the EDB model. The parameters m, K_0, and Q of the grain growth kinetics equation, i.e., Equation (58), have to be input into the EDB model to perform the Monte Carlo simulation.

The grain growth kinetics were calculated from the grain size data in isothermal grain growth experiments. The grain growth data in the experiments are summarized in Table 4. To fit the grain growth data into the power law of grain growth kinetics, i.e., Equation (6), a further mathematical analysis was necessary. Theoretically, when L_0 approached zero, the Equation (54) could be simplified as

$$L^m = K_0 \exp(-\frac{Q}{RT})t \qquad (60)$$

Assuming that the grains start growing from zero-sized initial grains at $t = \tau$, then Equation (60) should be rewritten as

$$L^m = K_0 \exp(-\frac{Q}{RT})(t-\tau). \qquad (61)$$

Noting that

$$K = K_0 \exp(-\frac{Q}{RT}) \qquad (62)$$

Equation (61) was rewritten as

$$\ln(L) = [\frac{1}{m}\ln(K)] + \frac{1}{m}\ln(t-\tau). \qquad (63)$$

Table 4. Experimental results on grain growth kinetics of 0.2% Cu-Al

Sample ID	Temperature (C)	Time (sec)	L_T (mm)	Mean P_T with 95% C.I.	Mean grain size (mm)
201	540	60	10.5	22.79 ± 0.05	0.460 ± 0.001
202	540	30	10.5	24.41 ± 0.02	0.430 ± 0.001
203	540	120	10.5	17.79 ± 0.04	0.590 ± 0.001
204	540	10	10.5	43.75 ± 0.07	0.240 ± 0.001
205	540	300	10.5	14.61 ± 0.02	0.720 ± 0.001
206	540	600	10.5	11.94 ± 0.05	0.880 ± 0.004
211	500	60	10.5	31.80 ± 0.04	0.330 ± 0.001
212	500	120	10.5	24.40 ± 0.08	0.430 ± 0.001
213	500	30	10.5	41.85 ± 0.03	0.250 ± 0.001
214	500	300	10.5	18.10 ± 0.06	0.580 ± 0.002
215	500	600	10.5	16.68 ± 0.02	0.630 ± 0.001
221	450	30	10.5	not fully recrystallized	
222	450	60	10.5	not fully recrystallized	
223	450	120	10.5	36.83 ± 0.04	0.285 ± 0.001
224	450	300	10.5	28.78 ± 0.06	0.365 ± 0.001
225	450	600	10.5	24.13 ± 0.03	0.435 ± 0.001
231	400	300	3.44	15.64 ± 0.07	0.220 ± 0.003
232	400	120	3.44	20.22 ± 0.05	0.170 ± 0.001
233	400	600	10.5	37.58 ± 0.03	0.280 ± 0.001
234	400	3600	10.5	24.40 ± 0.08	0.430 ± 0.001

This was equivalent to a linear equation: $y = a + bx$, where $y = \ln(L)$, $a = \ln(K)/m$, $b = 1/m$ and $x = \ln(t-\tau)$. τ was the assumed time offset between zero-sized grains to the initial experimental grains. Figure 12 shows the relationship between τ and real time.

By assuming a τ value, the grain size data from the experiment were separately fitted into Equation (63) at each temperature by a least square regression method. To evaluate the regression results, a deviation function Δ was defined as

$$\Delta = \sum [(L_i)_{cal} - L_i]^2 \tag{64}$$

where $(L_i)_{cal}$ was the grain size calculated from the regressed equation, and L_i was obtained from the experiment data set. The equation that had the minimum Δ value was selected as the grain growth kinetics equation. Figure 13 shows the dependency of the deviation function Δ on τ in 0.2% Cu-Al alloy. The analysis results are listed in Table 5.

Table 5 Results of grain growth kinetics analysis for 0.2% Cu-Al alloy

Temperature, C	τ, seconds	K	m (= 1/n)	Δ, mm^2
400	64.0	8.9699×10^{-6}	4.09	8.4×10^{-5}
450	39.0	5.4971×10^{-5}	4.14	1.0×10^{-9}
500	21.5	2.6536×10^{-4}	4.33	1.7×10^{-3}
540	7.0	9.3902×10^{-4}	4.17	2.1×10^{-3}

Since K was a function of temperature and was defined in Equation (62), the activation energy Q = 36.14 Kcal and $K_0 = 3.99 \times 10^6$ could be obtained from a plot of ln(K) versus 1/T, as shown in Fig. 14. It was seen from Table 5 that m was not a strong function of the temperature. The variation of the grain growth exponent, m, was less than 5%. Therefore, it was reasonable to assume the m value was a constant. The mean value of m in Table 5 is 4.18.

Substituting m, K_0 and Q values into Equation (58) yielded

$$L^{4.18} = 3.99 \times 10^6 \exp(-\frac{36{,}140}{RT})t. \tag{65}$$

When the initial grain size was taken into account, the grain growth kinetics for the 0.2% Cu-Al alloy can be expressed as

$$L^{4.18} - L_0^{4.18} = 3.99 \times 10^6 \exp(-\frac{36,140}{RT})(t - t_0) \quad (66)$$

where L and L_0 (in mm) were the grain size at time (in seconds) t = t and t = t_0, R was gas constant (R = 1.987 cal/mol/K), and T (in K) was the temperature.

Figure 15 compares the grain sizes measured in the experiment to those calculated from Equation (66). It is obvious that the calculated grain size is in good agreement with the experimental data. Equation (66) is the required grain growth kinetics for the EDB model.

Welding Experiments

The power input in GTAW of the 0.2% Cu-Al alloy was 9.5 V × 80 A = 760 W. The measured thermal cycle in the sample is shown in Fig. 16. Since it was difficult to measure the temperature near the fusion line, the thermal cycle at the fusion line was assumed to have a similar shape as that at other positions. The peak temperature at the fusion line was taken as the alloy solidus from the Al-Cu phase diagram. The dashed line in Fig. 16 shows the assumed thermal cycle at the fusion line. The thermal cycles in Fig. 16 were used to calculate the grain growth simulation time in the HAZ of 0.2% Cu-Al alloy. The measured peak temperature in the sample is shown in Fig. 17 as a function of the distance from the fusion line.

As expected, significant grain growth took place in the HAZ near the fusion line. Figure 18 gives the grain structure in the cross section of the welded sample. The grain size gradient in the HAZ is shown in Fig. 19.

Simulations of Grain Growth

Application of the GBM model to isothermal grain growth in zone-refined tin.[54] The size of the simulation matrix was chosen as 500 × 500. A periodic boundary condition was used. The random numbers at the simulation matrix sites were between 1 and 100. As shown in Fig. 20, the grain growth kinetics in this simulation system were

$$L = 0.14\lambda(MCS)^{0.48} \tag{67}$$

where L was mean grain intercept and λ was the lattice site spacing. Equation (67) gave two simulation model constants, i.e., $K_1 = 0.14$ and $n_1 = 0.48$.

The relationship between real time-temperature and simulation time was obtained by substituting the following parameters into the GBM model: $K_1 = 0.14$, $n_1 = 0.48$, $\gamma = 0.164$ $J \cdot m^{-2}$[77], $A = 1$, $Z = 3.15 \times 10^{18}\ m^{-2}$, $V_m = 1.66 \times 10^{-5}\ m^3 \cdot mol^{-1}$, $N_a = 6.02 \times 10^{23}\ mol^{-1}$, $\Delta S_f = 3.4\ cal \cdot mol^{-1} \cdot K^{-1}$[78], $h = 6.624 \times 10^{-34}$ J·sec, $Q = 6000\ cal \cdot mol^{-1}$[12], $R = 2\ cal \cdot mol^{-1} \cdot K$, $L_0 = 0$, and $\lambda = 2 \times 10^{-4}$ m, i.e.,

$$(MCS)^{0.96} = 16500\exp(-\frac{3000}{T})t. \tag{68}$$

By using the isothermal grain growth data from Holmes et al.[12], the isothermal grain growth of tin was simulated at 167 C, 185 C and 220 C. Figure 21 shows the comparison of simulated grain sizes to the experimental results. The simulated grain size was in agreement with experimental grain size. The simulated grain structures generated by this technique for an isothermal process are shown in Fig. 22.

Application of the EDB model to the heat treatment of a titanium alloy (continuous heating).[53]

Semiatin *et al.*[79] analyzed the kinetics of beta grain growth during rapid, continuous heating of a conventional alpha-beta titanium alloy of composition 6.4% Al, 3.3% Mo, 1.6%

Zr, 0.28% Si, and balance Ti. The alloy was resistance heated at constant rates of 10, 25, 100 and 300 C/sec to temperatures in the range (1050 C ≤ T ≤ 1200 C) and then immediately quenched in water. All treatments produced fully annealed beta microstructures. According to their analysis, the grain growth kinetics of the beta phase could be expressed as

$$L^2 - L_o^2 = 2.02\times10^{12}\exp(-\frac{251{,}000}{RT})t \qquad (69)$$

where L was the grain size, L_0 was the initial grain size (3.5 μm), R was the gas constant, t was the time, and T was the temperature.

When Equation (69) was equated to Equation (67) and compared with Equation (59), the following relationship was obtained

$$(MCS)^{0.96} = \frac{625}{\lambda^2}+\frac{1.03\times10^{14}}{\lambda^2}\Sigma[\exp(-\frac{251{,}000}{RT_i})t_i] \qquad (70)$$

where λ was the lattice site spacing in μm, and R was the gas constant (8.31 J/mol/K).

The grain growth was simulated[53] using Equation (70). The following simulation system was selected: 500 × 500 simulation matrix with 1-100 random numbers, and a periodic boundary condition. When the heating rate was 10, 25, 100 and 300 C/sec, λ was taken as 5, 3.25, 1.7 and 1 μm, respectively. Figure 23 shows the grain size for both the simulation and the experimental[80] data. It was found that the simulated grain growth was in good agreement with the experiment results. Examples of the simulated grain structures when heating at a rate of 25 C/sec are shown in Fig. 24.

Application of EDB model to grain growth in HAZ of 0.2% Cu-Al alloy. The initial grain size of the 0.2% Cu-Al alloy was about 47.5 μm. To ensure the grain size range in the HAZ simulation would be correctly mapped to a 800 × 600 simulation matrix, the lattice site spacing of the simulation matrix was selected as 10 μm. This simulation matrix represented

a physical area of 8000 μm × 5200 μm. Since the grain growth at locations where the peak temperature was high would be quite different from that where the peak temperature was low, half periodic boundaries were used, i.e., only the matrix boundaries parallel to the thermal gradient were wrapped. The orientation numbers ranged between 1 and 10,000. A Radhakrishnan-Zacharia Monte Carlo simulation procedure[52] was used to accelerate the simulation. The reorientation probability was calculated from Equation (22). The simulated grain growth kinetics in this simulation system was expressed as

$$L = 0.86\lambda (MCS)^{0.482}. \tag{71}$$

Figure 25 plots the simulated grain growth kinetics in this simulation system.

The isothermal grain growth kinetics in 0.2% Cu-Al alloy were determined by experiments, as expressed by Equation (66). The simulation time was related to real time-temperature by substituting the parameters in Equations (66) and (71) into the EDB model which was given by

$$(MCS)^{0.624} = 1266 \cdot \sum 4.28 \times 10^{16} \exp(-\frac{18188}{T(t)}) \Delta t. \tag{72}$$

The required simulation time at each simulation site was obtained by applying the thermal cycles shown in Fig. 16 to Equation (72) (see Fig. 26). Figure 27 shows the simulated grain structure in the HAZ of 0.2% Cu-Al after welding. A photograph of the grain structure in the as-weld HAZ is shown in Fig. 27 for comparison. Figure 28 plots the grain size measurements for both the simulated HAZ and the real HAZ. Figures 26 and 27 show the good accuracy obtained by the Monte Carlo simulation technique.

Grain growth with Zener pinning of second phase particles[58]. Typical evolutions of grain structure in the simulation of grain growth with second phase particles are shown

in Fig. 29. If the second phase particles were initially located only at grain boundaries, the grain boundaries would break away from a few pinning particles, as shown in the left column of Fig. 29. When the second phase particles were initially located randomly in the simulation matrix, all but a few of the particles became attached to grain boundaries at the final pinned stage, as shown in the right column of Fig. 29. The end results of the grain structure in each case was about the same. Figure 29 shows only a small portion (about 4%) of the total simulation matrix so that the detail of the precipitate-grain boundary contact could be enlarged for visual examination. However, all measurements and calculations of the microstructure were performed on the entire simulation matrix.

It was found that the grain size increased during the simulations until a stable size was reached. The grain growth kinetics for a second phase area fraction of 0.01 is shown in Fig. 30. It is interesting to note that no matter how the second phase particles were initially distributed in the simulation matrix, the grain growth kinetics were similar if the particle size and area fraction were the same. It can also be seen that both the simulation time required for a pinned structure and the pinned grain size increase with particle size for a given area fraction of second phase. As expected, larger particles had less pinning effect than smaller particles for a fixed second phase fraction. As shown in Fig. 31, for a single particle size, the larger the area fraction, the greater the pinning effect.

Figure 32 shows a plot of (D/r) against f. The mean grain size D was the mean intercept in the pinned grain structure. A best curve fitting gave the relationship between D/r and f as

$$\frac{D}{r} = 1.18 f^{-0.52}. \qquad (73)$$

The exponent of f in Equation (73) was similar to Srolovitz's[45].

The degree of contact also continued to increase in the simulations until it reached a stable value. Figure 33 shows the simulation results with 1-cell-sized particles. At the pinned state, the values of the degree of contact were constant with constant area fraction of second phase particles despite differences in the initial locations of particles. When the area fraction reached 0.15, almost all grain boundaries were covered by the second phase particles. In this case, the grain size and the degree of contact remained unchanged during the simulation, and the grain structure was frozen.

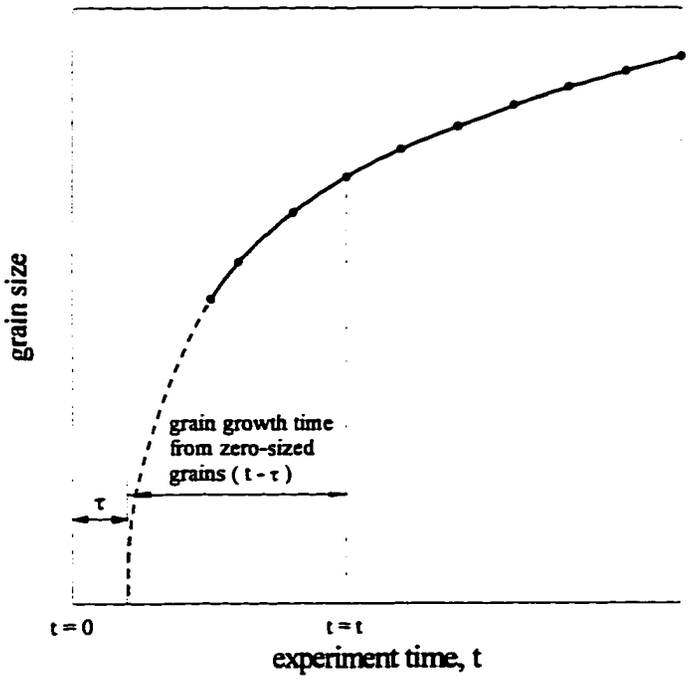

Fig. 12. The assumed time offset, τ.

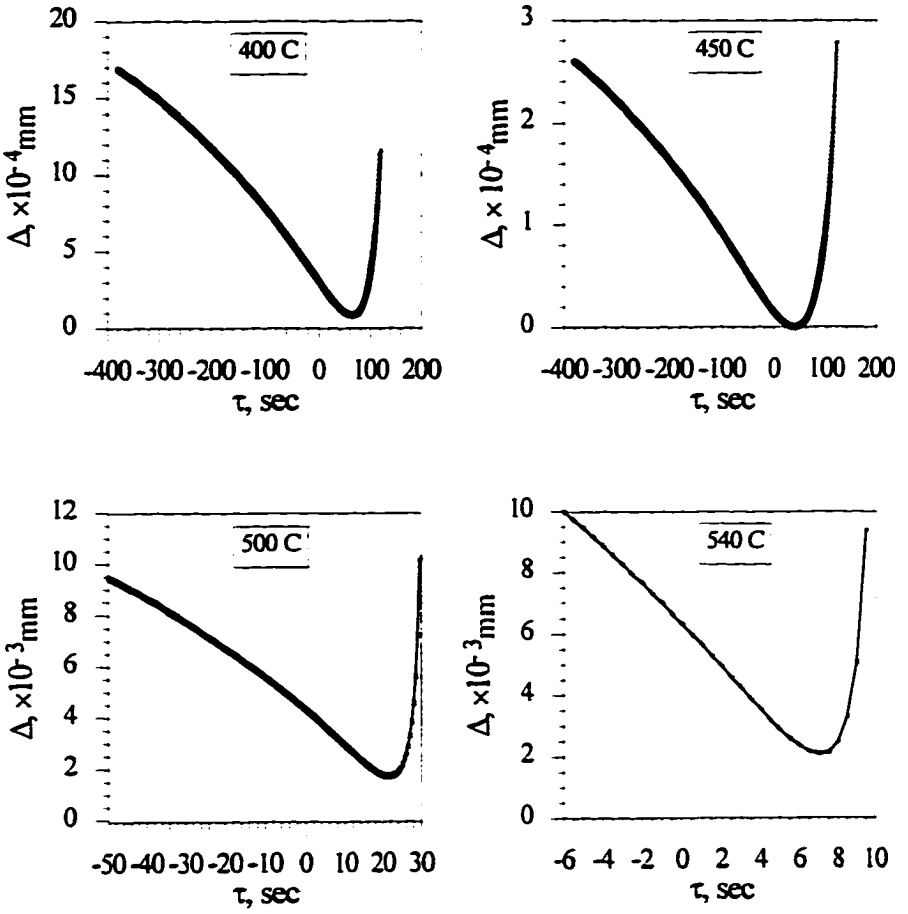

Fig. 13. The deviation function as a function of assumed time offset, 0.2% Cu-Al.

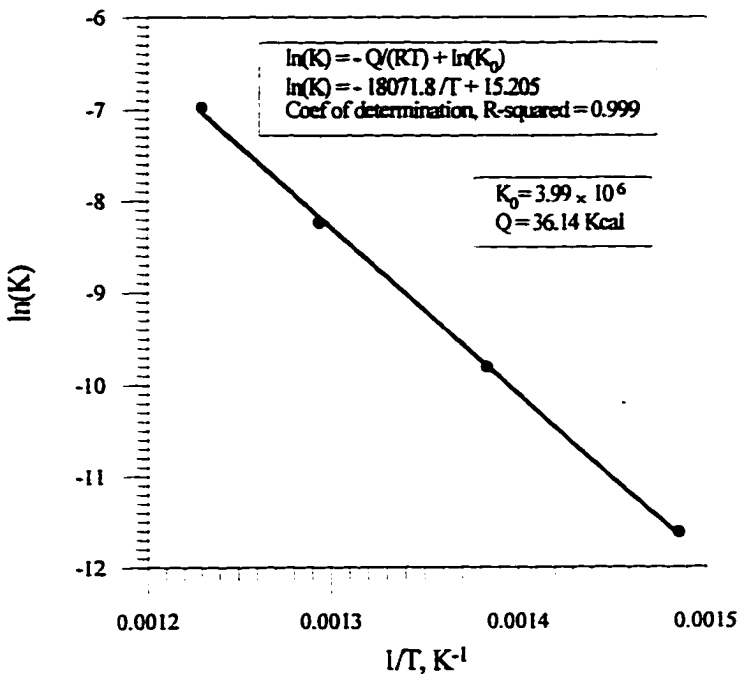

Fig. 14. Determination of K_0 and Q in grain growth kinetics, 0.2% Cu-Al.

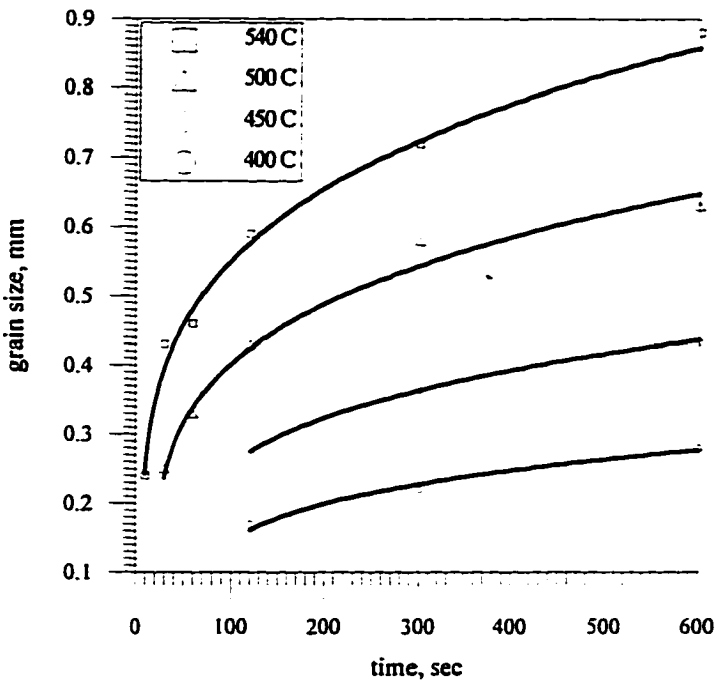

Fig. 15. Isothermal grain growth kinetics, 0.2% Cu-Al.

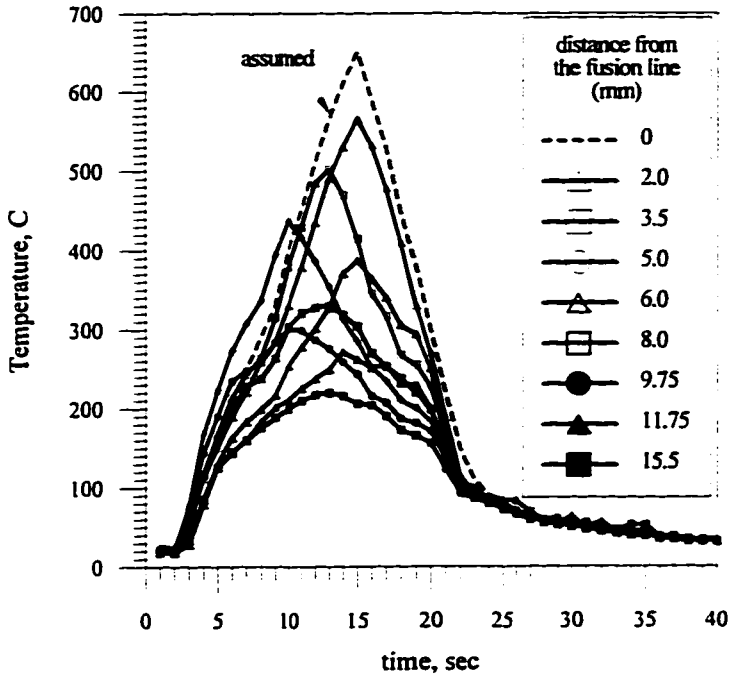

Fig. 16. The thermal cycles in the HAZ of 0.2% Cu-Al plate, GTAW welding, arc speed: 7.5 ipm, power input: 760 W.

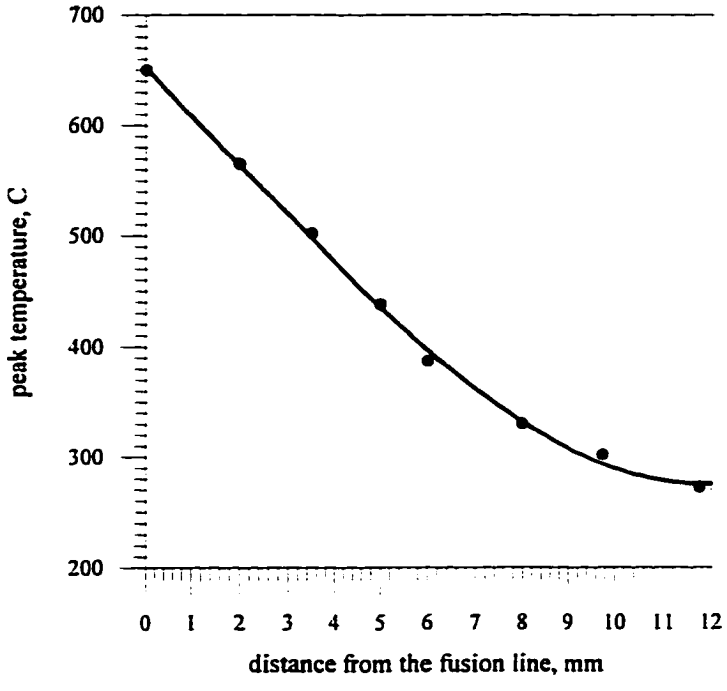

Fig. 17. The peak temperature gradient in the HAZ of 0.2% Cu-Al.

Fig. 18. Real grain structure in the weld of 0.2% Cu-Al.

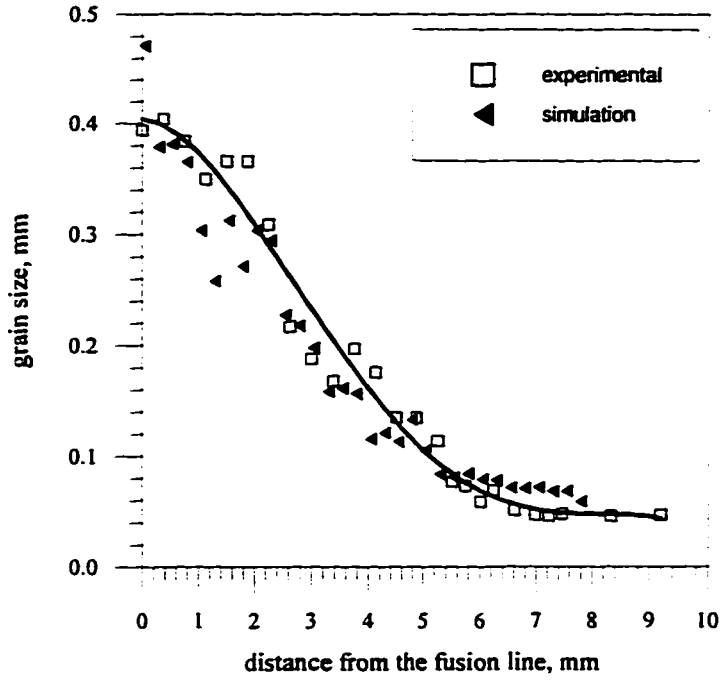

Fig. 19. Grain size gradient in the HAZ of 0.2% Cu-Al.

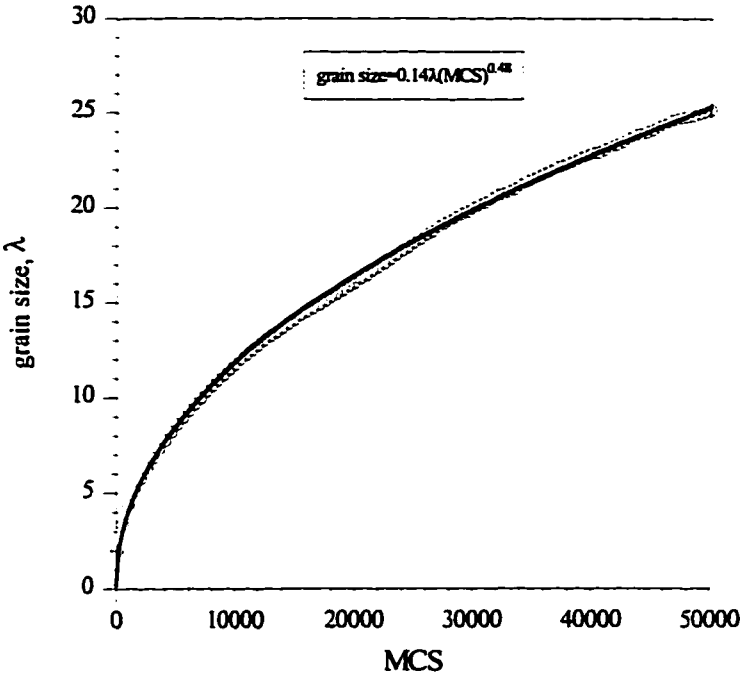

Fig. 20. Simulated grain growth kinetics, simulation matrix size: 500 × 500, random numbers: 1-100.

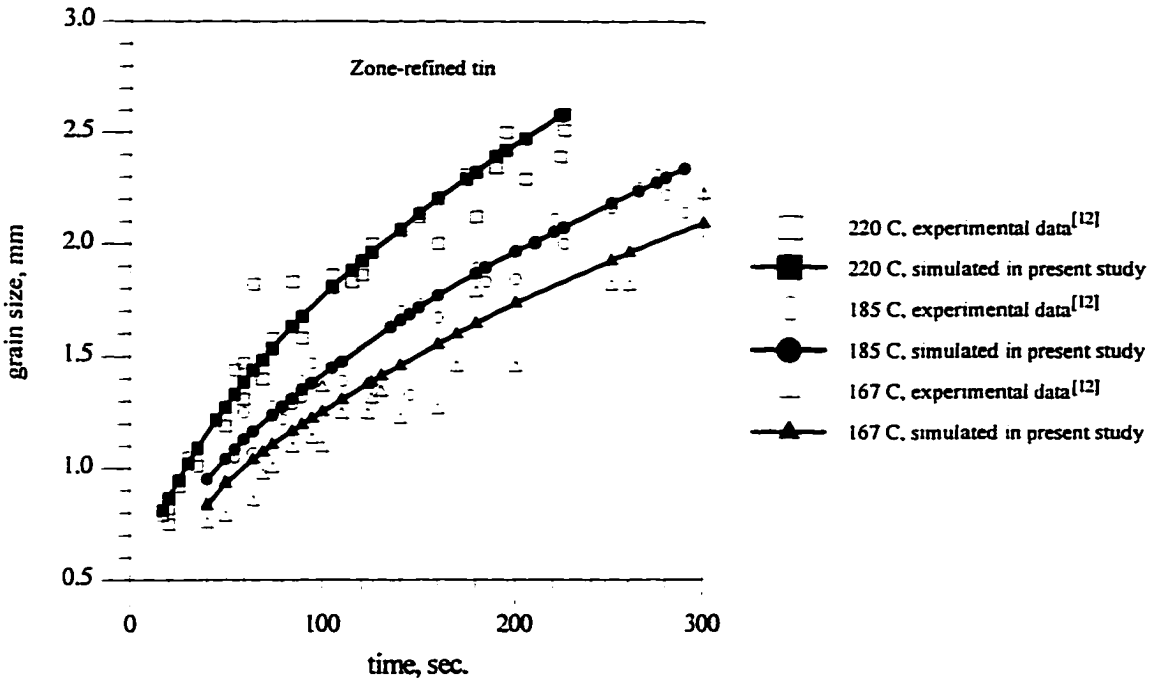

Fig. 21. Comparison of simulated grain size with real grain size in isothermally heated zone-refined tin.

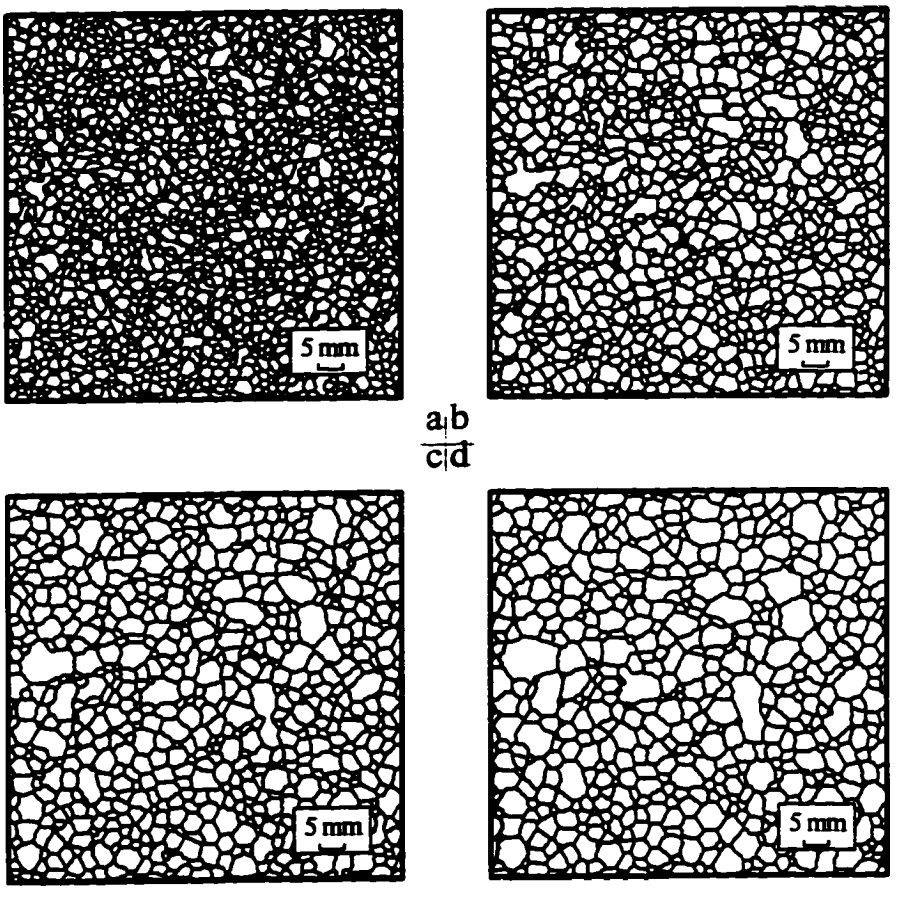

Fig. 22. Simulated grain structures in zone-refined tin, heated at 185 C for (a) 75 sec, (b) 150 sec, (c) 225 sec, and (d) 300 sec, by GBM model.

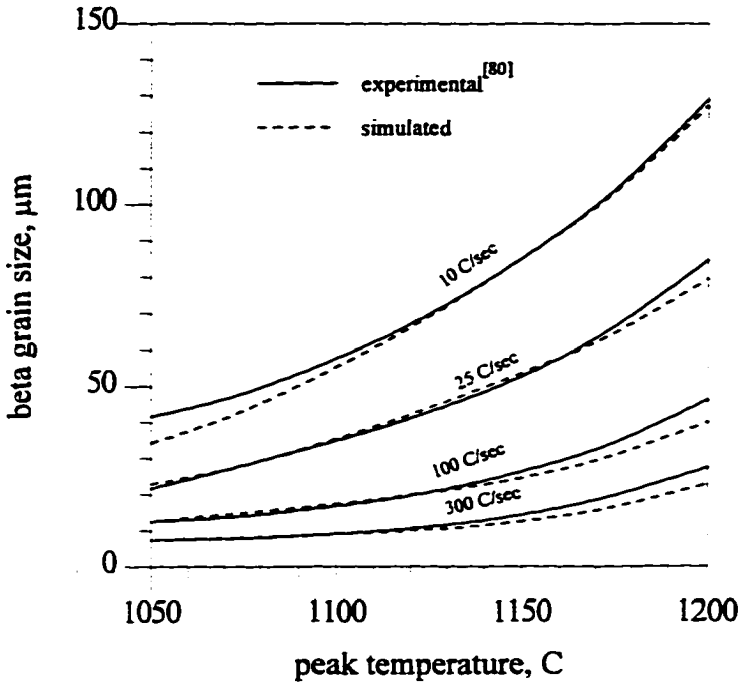

Fig. 23. Comparison of simulated grain size with real grain size in a continuously heated Ti-alloy.

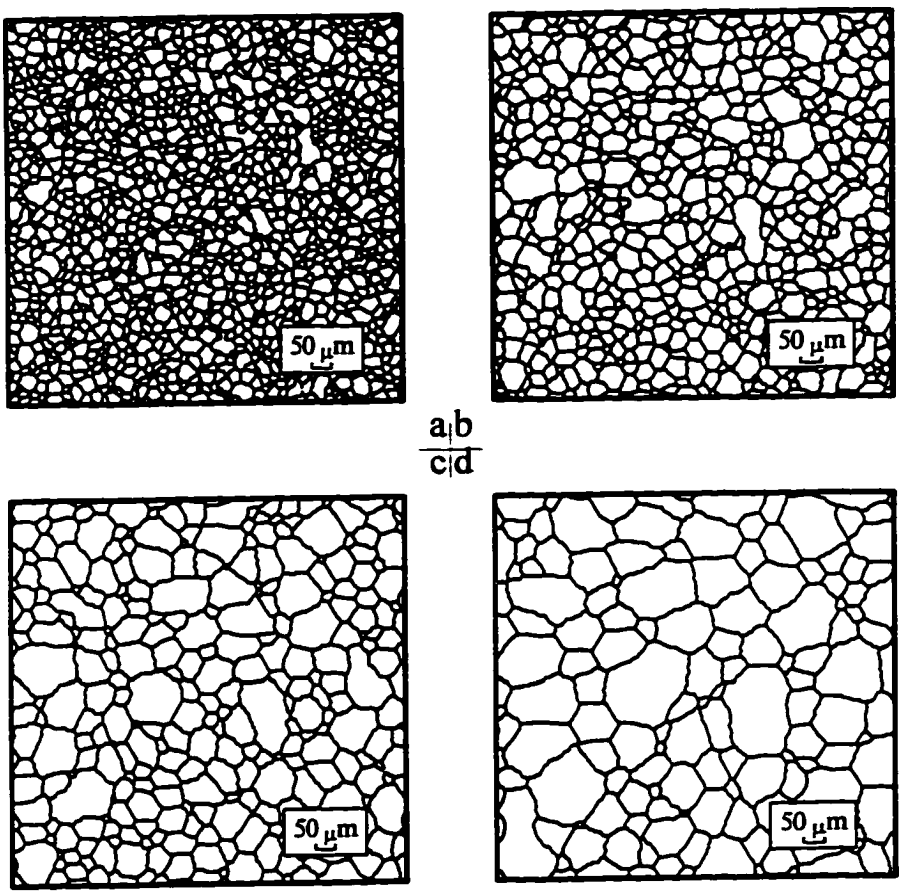

Fig. 24. Simulated β grain structures in a continuously heated Ti-alloy. Heating rate: 25 C/sec, peak heating temperature: (a) 1050 C, (b) 1100 C, (c) 1150 C, and (d) 1200 C, by EDB model.

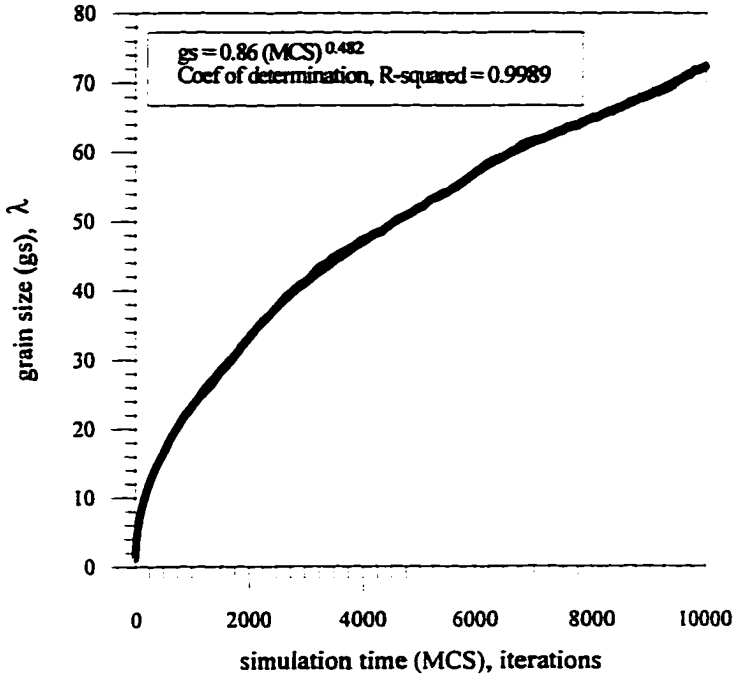

Fig. 25. Simulated grain growth kinetics, simulation matrix size: 800 × 600, random numbers: 1-10,000.

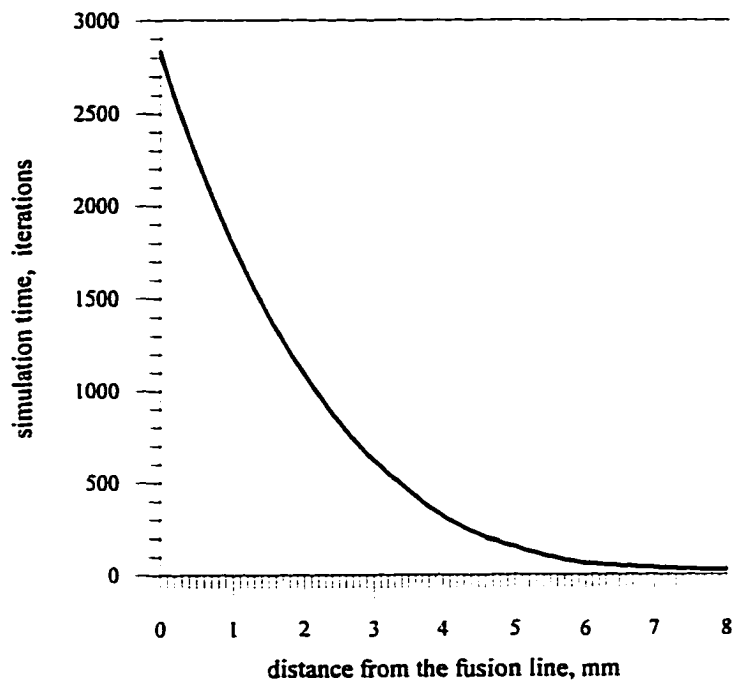

Fig. 26. The simulation time in the HAZ of 0.2% Cu-Al.

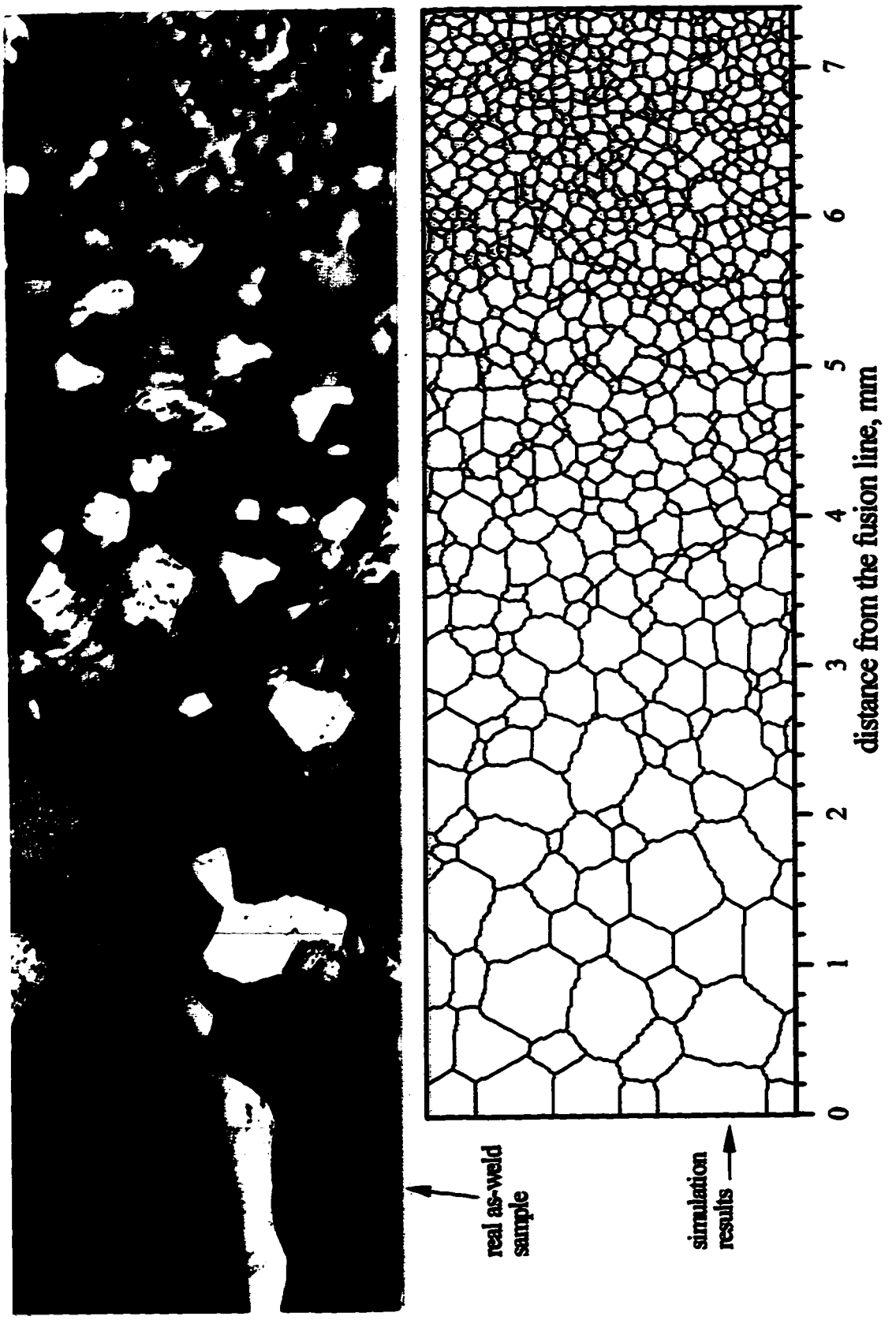

Fig. 27. Simulated and real grain structures in the HAZ of 0.2% Cu-Al alloy.

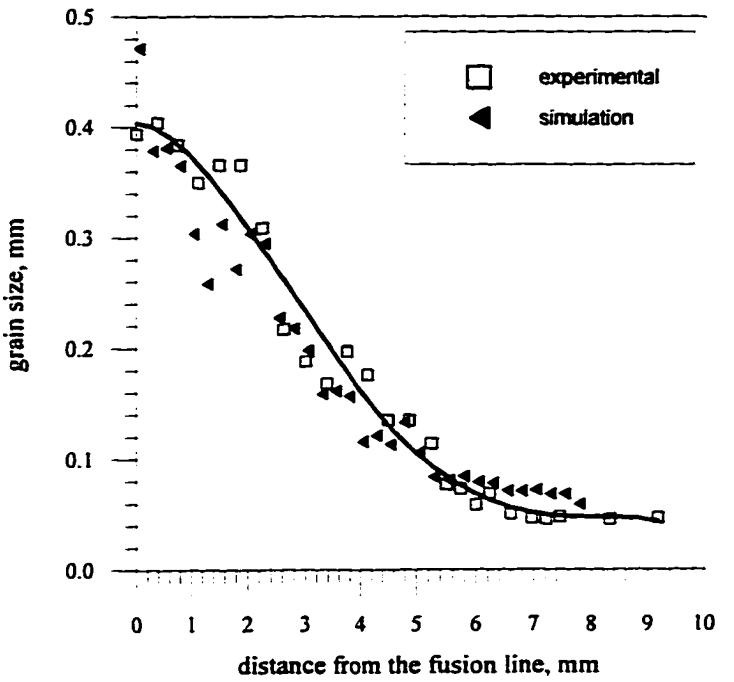

Fig. 28. Real grain size and simulated grain size in the HAZ of 0.2% Cu-Al alloy.

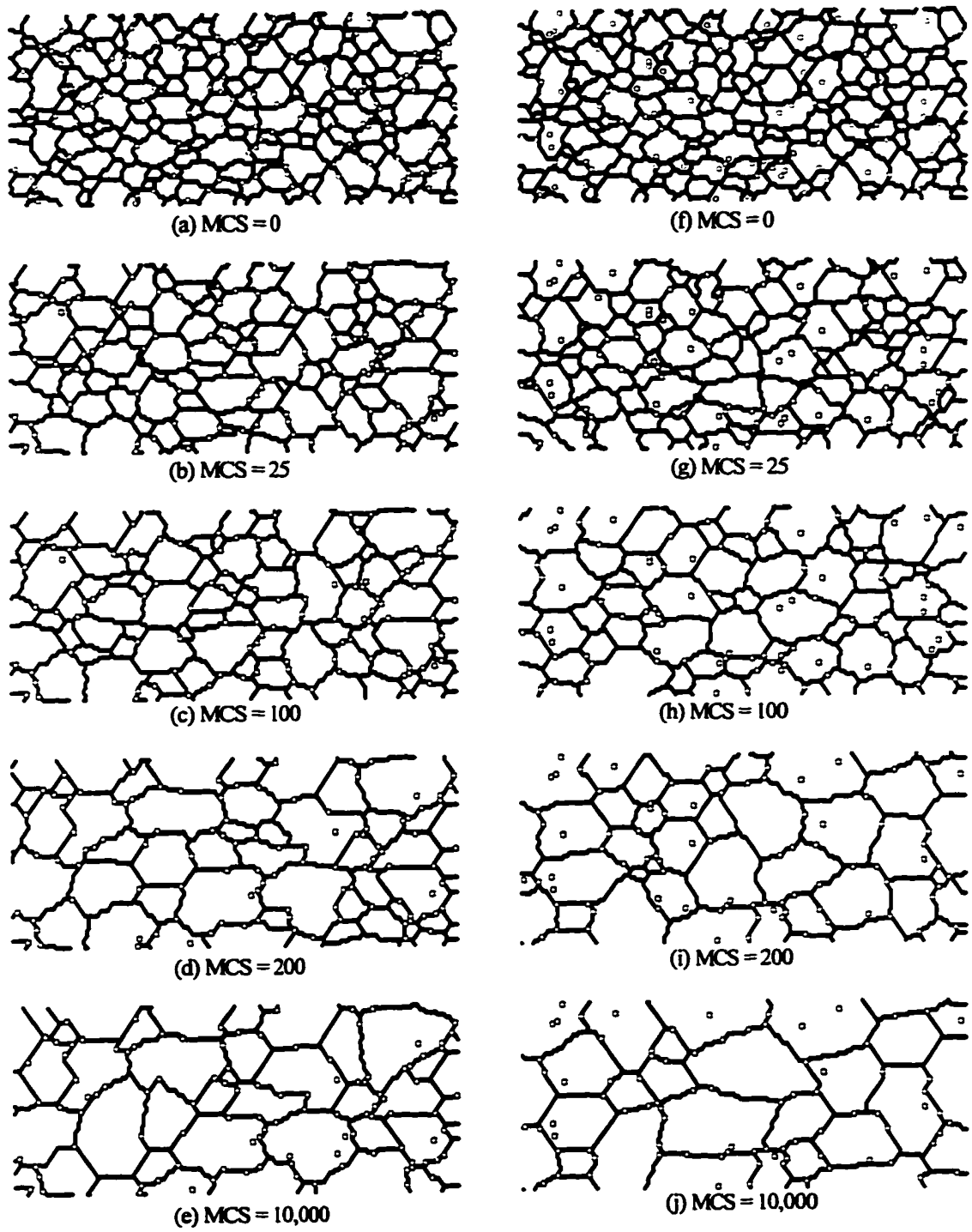

Fig. 29. Grain structure evolutions in the simulation, f = 0.01, initial location of the second phase particles: (a)-(e) only on grain boundaries; (f)-(j) randomly in the simulation matrix.

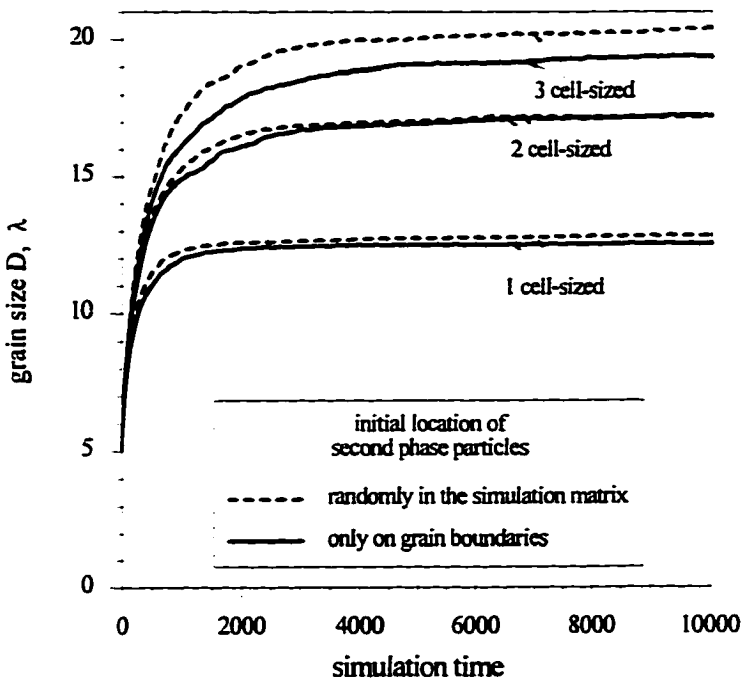

Fig. 30. Effect of size and initial location of second phase particles on grain growth kinetics, f = 0.01.

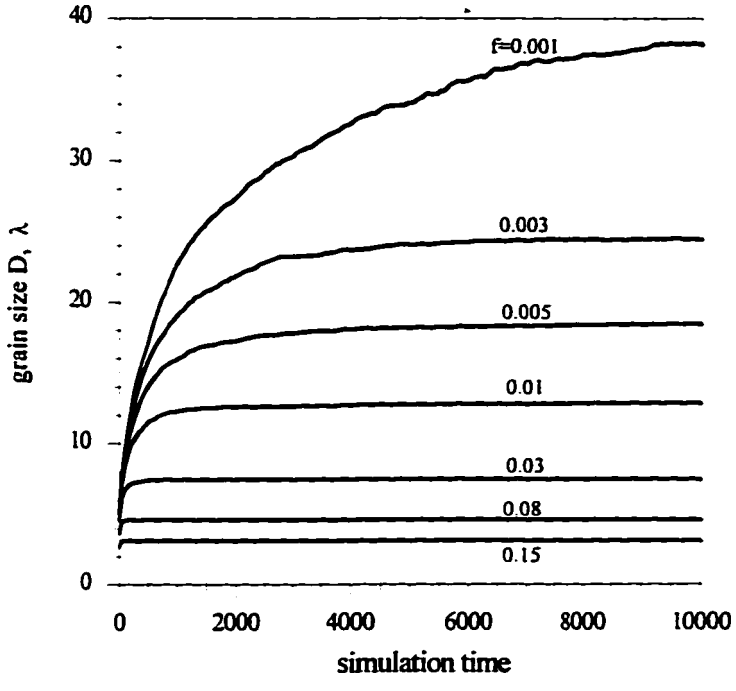

Fig. 31. Grain growth kinetics with 1-cell-sized second phase particles, initially located randomly in the simulation matrix.

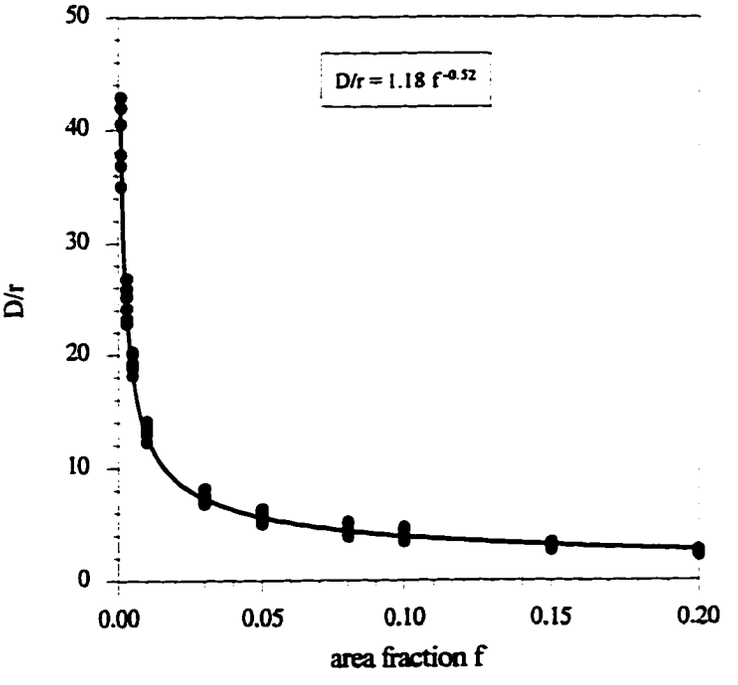

Fig. 32. Relationship between D/r and f.

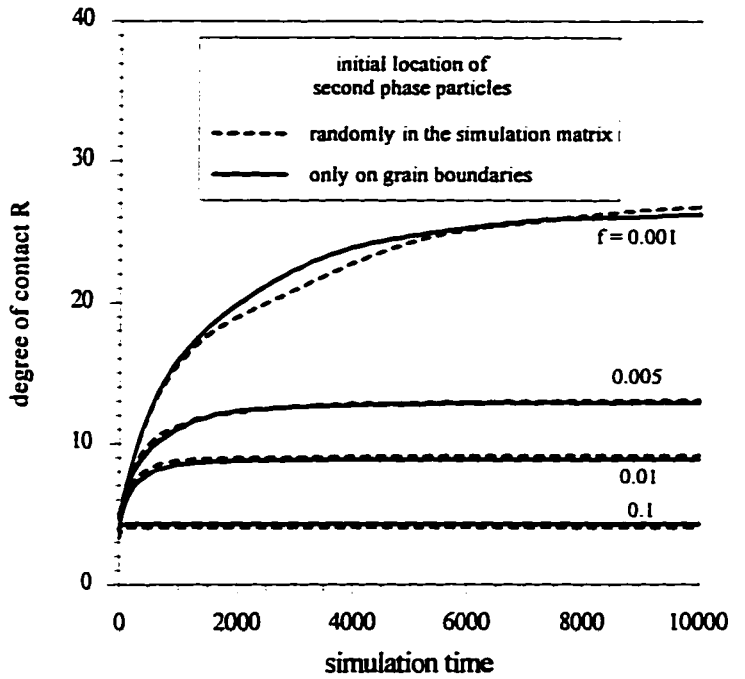

Fig. 33. Change in degree of contact during simulation, 1-cell-sized particles.

DISCUSSION

Selection of Monte Carlo Simulation System

The Monte Carlo simulation system includes the site arrangement, the amount of random numbers N, the dimension of the simulation matrix, the site spacing λ, and the calculation of switching probability.

The site arrangement in the simulation matrix could be triangular, square, or other shapes. Anderson et al.[51] showed that if the simulation system adopted a square site arrangement, the grain size and the morphology appeared to be evolving towards a "frozen-in" configuration where all boundaries met at 90° or 180° and had no curvature. The grain growth rate was very slow in such a system. When the amount of random numbers N exceeded 3 ($N \geq 3$), the time exponent in simulated grain growth kinetics approached zero ($n_1 \sim 0$). Therefore, a square site matrix is not a good candidate for grain growth simulation in metal and metallic alloy systems. On the other hand, the matrix with a triangular site arrangement showed continuing grain growth throughout the simulation. The time exponent in simulated grain growth kinetics is acceptable, as shown in Figs. 20 and 25.

Given a site arrangement, the simulated grain growth kinetics in the Monte Carlo simulation depend on the total number of random orientation numbers used in the simulation. Figure 34 shows such a dependence in a triangular site arrangement system. As we know, a grain is defined as one cluster of adjacent lattice sites with the same orientation number, and grain boundaries only exist between two lattice points with different orientation numbers. Grain coalescence and, hence, grain growth is quicker with fewer orientation

numbers. In simulation of normal grain growth with equiaxed grains, such as in metals or their alloys, the total number of random numbers, N, should be large enough to produce equiaxed grains in the simulation by preventing too much grain coalescence.

In Monte Carlo simulation, the lattice sites are treated as a block of physical area (in 2-D) in the material. In order to achieve efficient simulation of grain growth, two factors need to be considered. One is the number of Monte Carlo simulation iterations required by a given metallurgical process. The other is the simulation accuracy. Careful selection of the lattice site spacing plays an important part in these respects. In the present work, the number of simulation iterations used for grain growth went from 1,000 to 20,000 iterations. In this simulation time range, the relation of simulation time to real time-temperature can be accurately represented by Equations (67) and (71). The lattice site spacing should be adjusted carefully to ensure that the number of MCS lies in this range. If the selected lattice site spacing is too large, the number of MCS will be too few to give good agreement of simulated grain size with Equations (67) and (71). On the other hand, if the selected lattice site spacing is too small, the required number of MCS might be too large to run in the computer.

Application of the Two Models

In the application of Monte Carlo simulation to real metallurgical processes, the real time-temperature has to be converted to simulation time. The simulated grain growth kinetics will be quite different if different N, the total number of random orientation numbers, is used in the simulation, as shown in Fig. 34. Therefore, the conversion of real time-temperature to simulation time in a model should include the information from the simulated grain growth kinetics. The two models in this work include the simulated grain growth kinetics through the model constants K_1 and n_1 in Equations (55), (56), (58), and (59). Thus, for the present

case, no matter how many random orientation numbers were chosen in the simulation, the simulation results would have been similar.

Generally, both GBM and EDB models can be used to simulate grain growth, regardless of grain size. When the isothermal grain growth kinetics of a material are available, the EDB model can be used to simulate grain growth in isothermal processes and continuous heating and/or cooling processes with good agreement with experimental results. It is not necessary that the isothermal grain growth kinetics be for single phases or pure materials. As long as the grain growth data for the system are sufficient, the EDB model can be used to simulate its grain growth. When the grain growth data for a material of interest are not sufficient, the GBM model is a good approach to grain growth simulation. Here, the physical properties of the material system must be available. One drawback to applying this model to material systems is that the grain growth time exponent n in the GBM model is assumed to be 0.5. However, an exponent of 0.5 has been found for only a few systems[12]. For most experimental data in the literature, n is about 0.3. Therefore, when the GBM model is applied to a material system whose grain growth exponent is far from 0.5, the simulation result may be significantly different from the experimental result.

Description of Grain Size in HAZ

The grain size in HAZ is usually not uniform. It varies with the heat input during the welding process and the alloy system of the welds. A combination of the maximum grain size, which always occurs near the fusion line, and the mean grain size gradient in HAZ would characterize the grain size in HAZ. For this purpose, the mean intercepts of grains with equal distance x from the fusion line is measured as a function of x. A maximum grain size can be easily determined from the measurement. The mean grain size can be illustrated

by a plot of grain size versus the distance from the fusion line. A value of mean grain size gradient can be calculated from the plot. In the welding experiment presented in this dissertation, the maximum grain size was 0.42 mm, and the mean gradient of grain size was about 0.06 mm/mm. It is expected that the maximum grain size increases with total heat input during welding. The mean grain size gradient is a function of thermal gradient in the HAZ. The steeper the thermal gradient, the steeper the mean grain size gradient. However, more sections in the as-weld sample might be needed to make the grain size measurement accurate.

Modification of Zener Pinning Model[58]

In two dimensions, the relationship between pinned grain size and the second phase particle size can be derived similarly to Zener's original model. The driving force of normal grain growth per unit length of grain boundary is

$$F_d = \frac{S}{\rho} \tag{74}$$

where S is the grain boundary line tension, and ρ is the radius of grain boundary curvature. As shown in Fig. 35, when a grain boundary intercepts a second phase particle at an angle θ and the contact angle between the particle and grain boundary is ψ, the retarding force to grain boundary migration due to the pull from the particle is

$$2(f_r) = 2[S\cos(\psi-\theta)] \tag{75}$$

When $\psi = \theta$, the retarding force reaches its maximum. The maximum retarding force per length of grain boundary is

$$F_r = 2(-f_r)_{max} n_L = 2Sn_L \tag{76}$$

where n_L is the number of second phase particles per length of grain boundary, and can be related to particle size (r) and area fraction on grain boundaries (f_{gb}) by

$$n_L = 2r\frac{f_{gb}}{\pi r^2} = \frac{2f_{gb}}{\pi r}. \tag{77}$$

Substitution of Equation (77) into Equation (76) yields

$$F_r = \frac{4Sf_{gb}}{\pi r}. \tag{78}$$

If the driving force is greater than the retarding force, i.e., $F_d > F_r$, the grains can continue to grow and the grain boundaries can break through the drag of second phase particles. When $F_d = F_r$, the grain will not grow any more, and the grain size becomes stable and pinned. The balance of the driving and retarding force yields the relationship between pinned grain size, particle size and area fraction of second phase:

$$\frac{\rho}{r} = \frac{\pi}{4}f_{gb}^{-1}. \tag{79}$$

When the degree of contact between grain boundaries and second phase particles is defined as the ratio of second phase area fraction on grain boundaries (f_{gb}) to that in the material (f), it is equivalent to the earlier definition if the average size of the particles on the grain boundaries is the same as in the matrix. The degree of contact (R) value for this condition can be expressed as

$$R = \frac{f_{gb}}{f}. \tag{80}$$

and assuming the mean curvature radius of grain boundaries is proportional to mean grain interception, i.e.,

$$\frac{D}{\rho} = \kappa. \tag{81}$$

Equation (79) can be rewritten as

$$\frac{D}{r} = \frac{\pi\kappa}{4}(Rf)^{-1}. \tag{82}$$

Applying Equations (80) and (81) to Zener's original model, i.e., Equation (14), and defining f_{gb} as the volume fraction of second phase on grain boundaries and f as that in the material, gives a modified pinning model for 3-D:

$$\frac{D}{r} = \frac{4\kappa}{3}(Rf)^{-1}. \tag{83}$$

From Equations (82) and (83), it can be seen that both 2-D and 3-D Zener pinning models have similar expressions except for the coefficient of the $(Rf)^{-1}$ term.

Comparison of Modified Zener Pinning Model with Simulation Results

When (D/r) was plotted against (Rf), as shown in Fig. 36, a relationship similar to Equation (82) was obtained

$$\frac{D}{r} = 1.16\,(Rf)^{-0.96}. \tag{84}$$

The exponent value of the (Rf) term, -0.96, in Equation (84) was very close to that in the modified Zener pinning model. This suggested that the simulation results confirmed the modified Zener pinning model.

The degree of contact between grain boundaries and second phase particles in the pinned structure was a function of the area fraction of second phase particles, as shown in Fig. 37. The best curve fitting of Fig. 37 was

$$R = 0.9f^{-0.48}. \tag{85}$$

It is obvious that Equation (84) can be obtained by the substitution of Equation (85) into Equation (73). Therefore, the exponent of f term in Zener's original model, i.e., Equation (14), would be different from -1 unless the degree of contact, R, is independent on f.

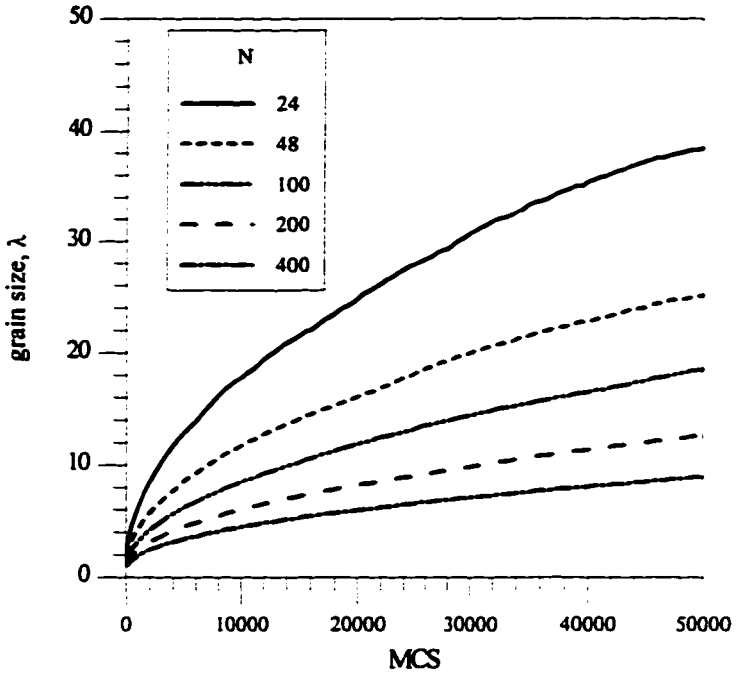

Fig. 34. Simulated grain growth kinetics with different N, the number of random orientation numbers.

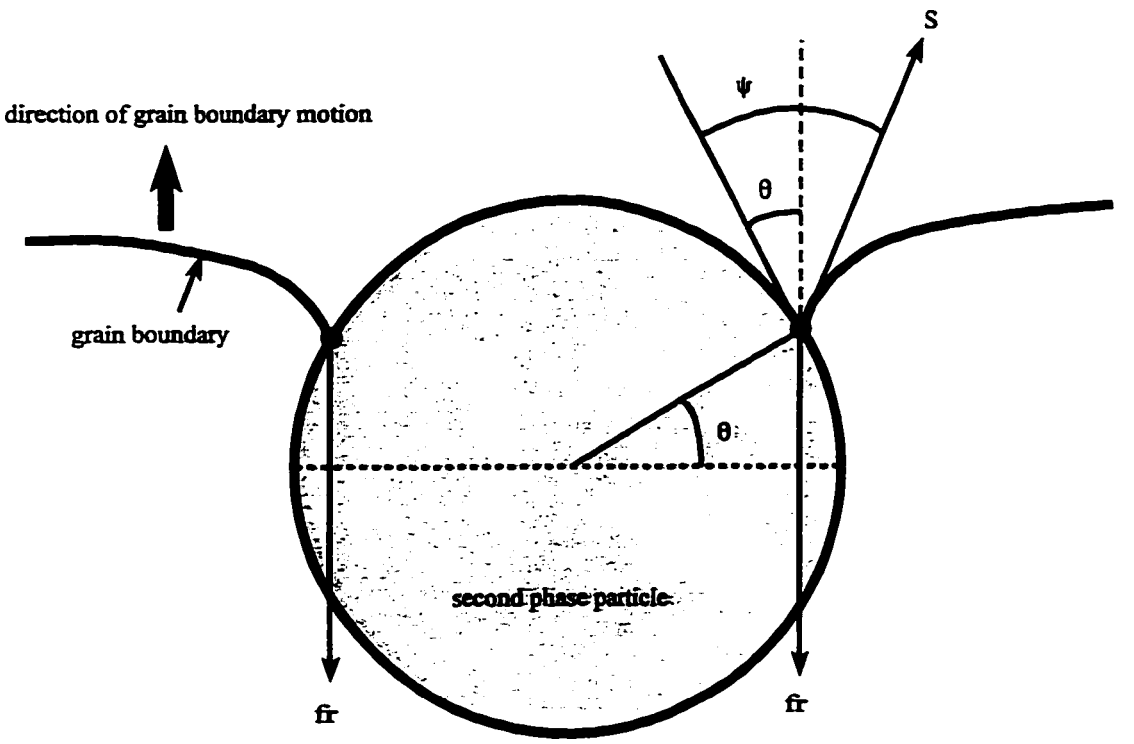

Fig. 35. The retarding force of a second phase particle on grain boundaries.

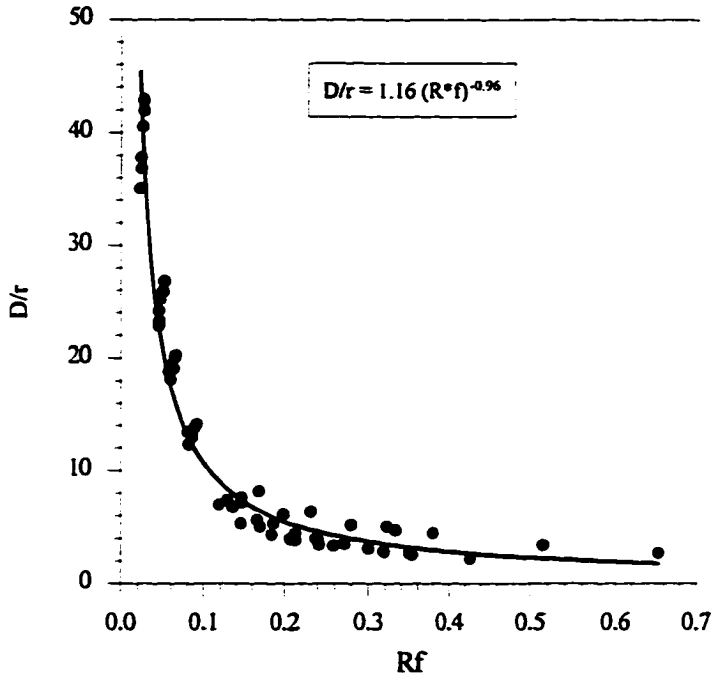

Fig. 36. Relationship between D/r and Rf.

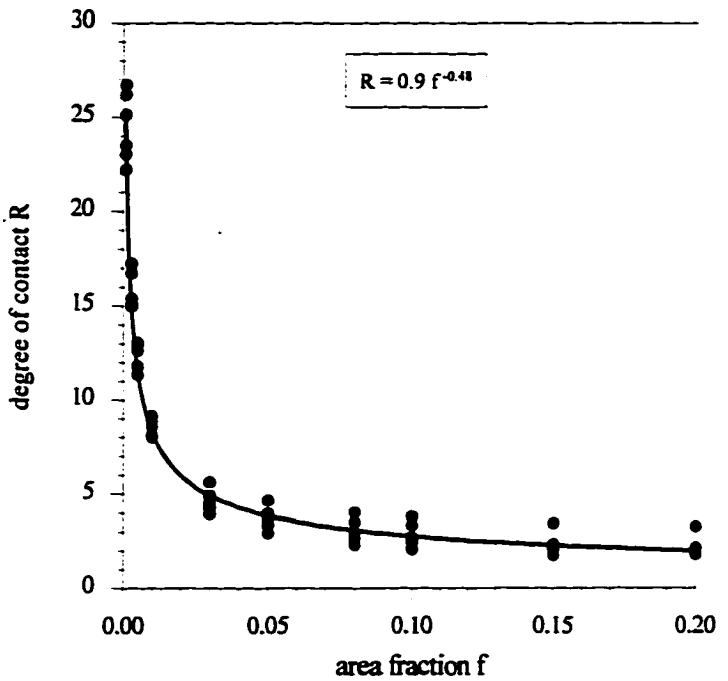

Fig. 37. Degree of contact versus area fraction of second phase particles.

CONCLUSIONS

Two real time-temperature models for Monte Carlo simulation of grain growth were developed that convert the real time-temperature to simulation time. When the experimental data on isothermal grain growth kinetics are available, the experimental data based model gives good results in the simulation. In cases where the experimental data is insufficient but data on physical properties is available, the grain boundary migration model can be used as an alternative to simulate grain growth.

The real time-temperature-based Monte Carlo simulation models were successfully applied to simulate normal grain growth in isothermal processes, continuous heating processes, and the HAZ of welds. The simulation results are in good agreement with experiment results. The Monte Carlo simulation technique can be used to simulate grain growth in various metallurgical processes.

A new mathematic method for analysis of experimental data on grain growth kinetics was proposed. The regression analysis developed in the dissertation gave values of Q and n which allowed good curve fitting of the experimental data to the power law of grain growth kinetics.

The maximum grain size near the fusion line and the gradient of mean grain size in HAZ may be used as characterization parameters of grain size in the HAZ of welds.

The Zener pinning model can be modified as $\frac{D}{r} = K(Rf)^{-1}$ by introducing the degree of contact between grain boundaries and second phase particles. Two-dimensional Monte

Carlo simulation of normal grain growth with second phase particles confirmed the modified pinning model.

REFERENCES

1. Atkinson, H. V., *Acta Metall.*, 1988, **36**, 469.

2. Beck, P. A., Kremer, J. C., Demer, L. J. and Holzworth, M. L., *AIME, Technical publication No. 2280, Metals Technology*, Sept. 1947, 1.

3. Burke, J. E. and Turnbull, D., *Progress in Metal Physics*, 1952, **3**, 220.

4. Smith, C. S., *Metal Interfaces*, ASM, Cleveland, OH, 1952, p.65.

5. Hillert, M., *Acta Metall.*, 1965, **13**, 227.

6. Rhines, F. N. and Craig, K. R., *Metall. Trans.*, 1974, **5A**, 413.

7. Doherty, R. D., *Metall. Trans.*, 1975, **6A**, 588.

8. Feltham, P., *Acta Metall.*, 1957, **5**, 97.

9. Louat, N. P., *Acta Metall.*, 1974, **22**, 721.

10. Cahn, J. W. and Padawer, G. E., *Acta Metall.*, 1965, **13**, 1091.

11. Morral, J. E. and Ashby, M. F., *Acta Metall.*, 1974, **22**, 567.

12. Holmes, E. L. and Winegard, W. C., *Acta Metall.*, 1959, **7**, 411.

13. Bolling, G. F. and Winegard, W. C., *Acta Metall.*, 1958, **6**, 283.

14. Gordon, P. and El-Bassyouni, T. A., *Trans. TMS-AIME*, 1965, **233**, 391.

15. Beck, P. A., Towers, J. Jr. and Manly, W. D., *AIME Trans.*, 1948, **175**, 162.

16. Hu, H. and Cline, R. S., *Trans. TMS-AIME*, 1968, **242**, 1013.

17. McGeary, R. K. and Lustman, B., *AIME Trans.*, 1953, **197**, 284.

18. Simpson, C. J., Aust, K. T. and Winegard, W. C., *Metall. Trans.*, 1971, **2**, 993.

19. Drolet, J. P. and Galibois, A., *Acta Metall.*, 1968, **16**, 1387.

20. Wang, J., Iwahashi, Y., Horita, Z. et al., *Acta Materialia*, 1996, **44**, 2973.

21. Burke, J. E., *AIME Trans.*, 1949, **180**, 73.

22. Miller, O. O., *Trans. ASM*, 1951, **43**, 260.

23. Detert, K. and Dressler, G., *Acta Metall.*, 1965, **13**, 845.

24. Hu, H., *Can. Metall. Q.*, 1974, **13**, 275.

25. Fasching, A. A., Edwards, G. R. and David, S. A., *Scripta Metall. Mater.*, 1994, **30**,1003.

26. Dunkerley, F. J., Pledger, F., Damiano, V. and Fulton, J., *AIME Trans.*, 1951, **191**, 1003.

27. Okazaki, K. and Conrad, H., *J. Metals*, March 1969, **21** , 35A.

28. Demer, L. J. and Beck, P. A., *AIME Trans.*, 1949, **180**, 147.

29. Wiener, G., *Trans, ASM*, 1952, **13**, 1169.

30. Anderson, M. P., Grest, G. S. and Srolovitz, D. J., *Scripta Metall.*, 1985, **19**, 225.

31. Hunderi, O., Ryum, N. and Westengen, H., *Acta Metall.*, 1979, **27**, 161.

32. Smith, C. S., *Trans AIME.*, 1948, **175**, 15.

33. Vandermeer, R. A. and Hu, H., *Acta Metall. Mater.*, 1994, **42**, 3071.

34. Grey, E. A. and Higgins, G. T., *Acta Metall.*, 1973, **21**, 309.

35. Hu, H. and Rath, B. B., *Metall. Trans.*, 1970, **1**, 3181.

36. Abbruzzese, G. and Lucke, K., *Acta Metall. Mater.*, 1986, **34**, 905.

37. Nes, K. J. and Ryum, N., *Acta Metall.*, 1975, **23**, 979.

38. Mistler, R. E. and Coble, R. L., *J. Am. Ceram. Soc.*, 1968, **51**, 472.

39. Zener, C., quoted by Smith, C. S., *Trans. TMS-AIME* , 1949, **175**, 15.

40. Porter, D. A. and Easterling, K. E., *Phase Transformations in Metals and Alloys*, Second Edition. Chapman & Hill, London, 1992, p.141.

41. Hassen, P., *Physical Metallurgy*, Van Norstrand, New York, 1978, p.362.

42. Shewmon, P. G., *Transformations in Metals*, McGraw-Hill, New York, 1969, p.122.

43. Hellman, P. and Hillert, M., *Scandinavian Journal of Metallurgy*, 1975, **4**, 211.

44. Hillert, M., *Acta Metall.*, 1988, **36**, 3177.

45. Srolovitz, D. J., Anderson, M. P., Grest, G. S. and Sahni, P. S., *Acta Metall.* 1984, **32**, 1429.

46. Doherty, R. D., Srolovitz, D. J. et al., *Scripta Metall.*, 1987, **21**, 576.

47. Anderson, M. P., Grest, G. S. et al., *Scripta Metall.*, 1989, **23**, 753.

48. Liu, Y. and Patterson, B. R., *Acta Metall. Mater.*, 1993, **41**, 2651.

49. Liu, Y. and Patterson, B. R., *Metall. Trans. A*, 1993, **24A**, 1497.

50. Liu, Y. and Patterson, B. R., *Acta Mater.* in press.

51. Anderson, M. P., Srolovitz, D. J., Grest, G. S. and Sahni, P. S., *Acta Metall.*, 1984, **32**, 783.

52. Radhakrishnan, B. and Zacharia, T., *Metall. and Mater. Trans.*, 1995, **26A**, 167.

53. Gao, J. and Thompson, R. G., *Acta Mater.*, 1996, **44**, 4565.

54. Srolovitz, D. J., Anderson, M. P., Sahni, P. S. and Grest, G. S., *Acta Metall.*, 1984, **32**, 793.

55. Srolovitz, D. J., Grest, G. S. and Anderson, M. P., *Acta Metall.*, 1985, **33**, 2233.

56. Rollett, A. D., Srolovitz, D. J. and Anderson, M. P., *Acta Metall.*, 1989, **37**, 1227.

57. Gao, J., Thompson, R. G., and Patterson, B. R., *Mathematics of Microstructure Evolution*, ed. Chen, L., Fultz, B., Cahn, J., Manning, J., Morral, J., and Simmons, J., EMPMD Monograph Series, TMS SIAM, 1996, p.31.

58. Gao, J., Thompson, R. G., and Patterson, B. R., *Acta Mater.*, in press.

59. Gao, J., Cao, Y. and Thompson, R. G., *Trends in Welding Research, 4th International Conference*, ed. Smartt, H. B., David, S. A., and Johnson, J. A., ASM International, 1996.

60. Srolovitz, D. J. et al., *Acta Metall.*, 1986, **34**, 1833.

61. Humphreys, F. J., *Mater. Sci. and Techno.*, 1992, **8**, 135.

62. Zhu, P. and Smith, W., *Acta Metall.*, 1992, **40**, 683.

63. Brown, S. G. R. and Spittle, J. A., *Mater. Sci. & Techno.*, April 1989, **5**, 362.

64. Ling, S. and Anderson, M. P., *J. of Metals*, 1992, **44(9)**, 30.

65. Ling, S., Anderson, M. P., Grest, G. S. and Glazier, J. A., *Materials Science Forum*, 1992, **94-96**, 39.

66. Radhakrishnan, B. and Zacharia, T., *International Conference on Modeling and Control of Joining Processes*, AWS, Miami, FL, October 1993.

67. Thompson, R. G. and Liu, Y., *International Conference on Modeling and Control of Joining Processes*, AWS, Miami, FL, October 1993.

68. Shen, Y., Monte Carlo Simulation of a Continuous Heating Process, Master's Thesis, the Department of Materials Science and Engineering, University of Alabama at Birmingham, 1993.

69. Shen, Y., Radhakrishnan, B. and Thompson, R. G., *Proceedings of the 3rd International Conference on Trends in Welding Research*, ed. David, S. A. and Vitek, J. M., ASM, Materials Park, OH, 1993.

70. Rosenthal, D., *Trans. ASME* , 1946, **68**, 849.

71. Christensen, N. et al., *Brit. Weld J.*, 1965, **54**, 54.

72. Hess, W. F. et al., *Weld J.*, 1943, **22**, s377.

73. Ashby, M. F. and Easterling, K. E., *Acta Metall.*, 1982, **30**, 1969.

74. Kou, S., *Metall. Trans. A*, 1981, **12A**, 2025.

75. Alberry, P. C., Chew, B. and Jones, W. K. C., *Metal Techno.*, 1977, **4(6)**, 317.

76. DeHoff, R.T. and Rhines, F.N., *Quantitative Microscopy*, McGraw-Hill, Inc, New York, 1968, p.30.

77. Chalmers, Bruce, *Principles of Solidification* John Wiley & Sons, Inc., New York, 1967, p.47.

78. Murr, L. E., *Interfacial Phenomena in Metals and Alloys*, Addison-Wesley, London, 1975.

79. Semiatin, S. L., Soper, J. C. and Sukonnik, I. M., *Scripta Metall. et Mater.*, 1994, **30**, 951.

80. Gordienko, A. I., Brun, M. Ya., Ivashko, V. V. and Elagina, L. A., *Titanium 1990: Products and Applications*, Titanium Development Association, Dayton, OH, 1990, p.726.

GRADUATE SCHOOL
UNIVERSITY OF ALABAMA AT BIRMINGHAM
DISSERTATION APPROVAL FORM

Name of Candidate Jinhua Gao

Major Subject Materials Engineering

Title of Dissertation Computer Simulation of Grain Growth in HAZ

Dissertation Committee:

, Chairman

Director of Graduate Program

Dean, UAB Graduate School

Date 9/4/97